

Molecular Electron Momentum Densities: Exploring Bond-directionality Principle in Field-free and Field-dressed Systems

Divya Suman

*A dissertation submitted for the partial fulfillment of BS-MS
dual degree in Science*



**INDIAN INSTITUTE OF SCIENCE EDUCATION AND
RESEARCH, MOHALI**

Department Of Chemical Sciences

May 2021

Certificate of Examination

This is to certify that the dissertation titled "**Molecular Electron Momentum Densities: Exploring Bond-directionality Principle in Field-free and Field-dressed Systems**" submitted by **Divya Suman (MS16090)** for the partial fulfilment of BS-MS dual degree program of the institute, has been examined by the thesis committee duly appointed by the Institute. The committee finds the work done by the candidate satisfactory and recommends that the report be accepted.

A black ink signature, possibly reading 'J. George', with a large diagonal stroke across it and the date '7/5' written below.

Dr. Jino George

A black ink signature, possibly reading 'S. Venkatramani', enclosed within a circular stamp.

Dr. Sugumar Venkatramani

A blue ink signature, possibly reading 'P. Balanarayan', written in a cursive style.

Dr. P Balanarayan

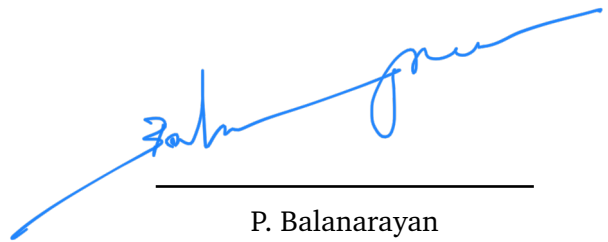
Declaration

The work presented in this dissertation has been carried out by me with Dr. P. Balanarayan at the Indian Institute of Science Education and Research, Mohali. This work has not been submitted in part or in full for a degree, a diploma, or a fellowship to any other university or institute. This thesis is a bonafide record of original work done by me and all sources listed within have been detailed in the References.



Divya Suman
(MS16090)

In my capacity as the supervisor of the candidates project work, I certify that the above statements by the candidate are true to the best of my knowledge.



P. Balanarayan
(Thesis Supervisor)

Acknowledgement

I would like to express my deepest gratitude to all those who have extended their generous help that made this work possible.

The first person I would like to express my gratitude to is my research supervisor, Dr. P. Balanarayan, for his support and encouragement throughout the project. I would also like to thank my project committee members, Dr. Jino George and Dr. Sugumar Venkatramani for reading drafts of this dissertation and providing many valuable comments that improved the contents of this dissertation.

My labmates, Sajan, Pankaj, Mishu, Prashant, Nitin, Naveen, Prateek, Alkit, Taseng, Harwinder, Kirti and Aman, have given me an environment in lab that I will cherish for a long time. I am immensely thankful to my mentor Mishu Paul for her constant guidance, inputs and discussion and also for reading numerous drafts of this thesis and providing valuable suggestions that improved this thesis. Without her expertise and encouragement, this thesis would not have been possible.

I would not have come this far without the love and support of my family. I am thankful to them for always having my back and for being supportive and encouraging at all times. Last but not the least, my friends Preeti, Kirti, Saurav, Shradha, Chahat, Anubhav, Bharath, Parth, Samyak, Sonell, Vishal, Abhishek, Sparsh, Hiral and Kimaya, for their company that helped me get through these five years.

We have no right to assume that any physical laws exist, or if they have existed up until now, that they will continue to exist in a similar manner in the future

- Max Planck

Contents

1	Introduction	1
1.1	Time-Independent Schrodinger Equation	1
1.2	Light matter interaction	2
1.2.1	Dipole Approximation	3
1.3	Electric Fields	4
1.3.1	Linear Homogeneous Electric Field	4
1.3.2	Polarized Laser Pulse	5
1.4	Scalar Fields	5
1.4.1	Electron density	6
1.4.2	Relationship between the position space and momentum space	7
1.4.3	Electron Momentum Density	7
1.5	Experimental measures of EMD	8
1.5.1	Compton Scattering	8
1.5.2	Positron Annihilation Experiment	9
1.6	Bond-directionality Principle	10
1.7	Thesis Outline	11
	References	13
2	Bond directionality in Electron Momentum Densities of Field-free Molecules	15
2.1	Dihydrogen (H_2)	15
2.1.1	Bond Directionality Principle : MO and VBT approximation .	15
2.1.2	Variation of EMD with increasing bond length	17
2.2	Trihydrogen cation (H_3^+)	21
2.2.1	Bond Directionality Principle : MO and VBT approximation .	21
2.2.2	Variation of EMD with increasing bond length	22
2.3	Ethylene Molecule	26
2.4	Bond-Oscillation Principle	27
2.5	Pair-wise momentum densities	27
2.5.1	Pair-wise momentum densities for H_3^+	29
2.5.2	Pair-wise momentum densities for Water	29

2.5.3	Pair-wise densities for Ethylene	30
3	Molecular Electron Momentum Densities of Field-dressed Systems	33
3.1	Complex Absorbing Potential (CAP)	34
3.2	Results and Discussion	34
3.2.1	H ₂	35
3.2.2	H ₃ ⁺	36
3.2.3	Water (H ₂ O)	39
3.2.4	Ethylene (C ₂ H ₄)	40
3.3	Conclusion and Future Prospects	43
	References	45

List of Figures

1.1	Potential energy curve for a system that is being subjected to a static electric field in Z-direction	4
1.2	Linearly polarised electric field with a sine squared envelope over it . .	5
1.3	Motion of a pendulum	7
1.4	A schematic diagram of Compton scattering. An incident photon of wavelength λ collides with an electron at rest. A new scattered photon of wavelength λ' emerges at an angle Φ and the electron recoils by an angle θ	9
1.5	Schematic for positron annihilation of an electron.	10
2.1	Ground state potential energy curve for H_2 , calculated using the full CI method with extended coemd-ref basis set.	18
2.2	A plot of (a) EMD and (b) Laplacian of EMD for H_2 at $ \vec{p} = 0$ as a function of the bond length. The values of both EMD and Laplacian at $ \vec{p} = 0$ was calculated using an in-house code for momentum space properties.	19
2.3	Isosurfaces of EMDs for H_2 for varying H-H bond length using the extended coemd-ref basis set, visualized using VMD at an isovalue of 0.05	20
2.4	Ground state potential energy curve for H_3^+ , calculated using full CI method with the extended coemd-ref basis set and RHF level of theory at each H-H bond length.	23
2.5	A plot of (a) EMD and (b) Laplacian of EMD for H_3^+ at $ \vec{p} = 0$ as a function of the bond length. The values of both EMD and Laplacian at $ \vec{p} = 0 $ was calculated using an in-house code for momentum space properties.	23
2.6	Isosurfaces of EMDs for H_3^+ at varying H-H bond length using the coemd-ref basis set along the restricted Hartree-Fock level of theory, visualized using VMD. The isovalues given in the figure are in a.u. . . .	25
2.7	(a) Isosurface for the total momentum density, (b) Isosurface of the Laplacian of the EMD and (c) Isosurfaces for the pairwise momentum densities of different pairs of H_3^+ . All the given isovalues are in a.u. .	29

2.8	(a) Isosurface for the total momentum density, (b) Isosurface of the Laplacian of the EMD, (c) Isosurfaces for the pairwise momentum densities of different pairs and (d) Isosurface of the bare-nuclear potential of H ₂ O. All the given isovalues are in a.u.	30
2.9	(a) Isosurface for the total momentum density, (b) Isosurface of the Laplacian of the EMD, (c) Isosurfaces for the pairwise momentum densities of different pairs and (d) Isosurface of the bare-nuclear potential of C ₂ H ₄ . All the given isovalues are in a.u.	31
3.1	(a) Geometry of H ₂ molecule. The black arrow denotes the direction in which the laser is induced. (b) Variation of $\gamma(\vec{0})$ with optical cycle in the presence of a linearly polarized Laser, along Z-direction. The x-axis represents the no. of optical cycles and the y1- and y2- axis represent EMD, $\gamma(\vec{0})$ (in red) and the energy of the pulse (in purple) in a.u., respectively. The electric field runs for 12 optical cycles and the pulse is ended after the 6 th optical cycle, with intensity, $\epsilon = 0.25$ a.u., $\omega = 0.21$ a.u., quiver distance, $\alpha_o = 5.668934$ a.u., with the CAP box size set to 20,26,26	35
3.2	Variation of the laplacian, $\nabla^2\gamma(\vec{0})$, of EMD for H ₂ , with optical cycle in the presence of a linearly polarized Laser, along Z-direction. The x-axis represents the no. of optical cycles and the y1- and y2- axis represent $\nabla^2\gamma(\vec{0})$ (in red) and the energy of the pulse (in purple) in a.u., respectively and intensity, $\epsilon = 0.25$ a.u.	36
3.3	(a) Geometry of H ₃ ⁺ molecule. The black arrow denotes the direction in which the laser is induced. (b) Variation of $\gamma(\vec{0})$ with optical cycle in the presence of a linearly polarized Laser, along X-direction. The x-axis represents the no. of optical cycles and the y1- and y2- axis represent EMD, $\gamma(\vec{0})$ (in red) and the energy of the pulse (in purple) in a.u., respectively. The electric field runs for 12 optical cycles and the pulse is ended after the 6 th optical cycle, with intensity, $\epsilon = 0.25$ a.u., $\omega = 0.21$ a.u., quiver distance, $\alpha_o = 5.668934$ a.u., and (c) with intensity, $\epsilon = 0.75$ a.u., $\omega = 0.21$ a.u., quiver distance, $\alpha_o = 17.007$ a.u., with the CAP box size set to 10,15,15.	37
3.4	Variation of the laplacian, $\nabla^2\gamma(\vec{0})$, of EMD for H ₃ ⁺ , with optical cycle in the presence of a linearly polarized Laser, along X-direction. The x-axis represents the no. of optical cycles and the y1- and y2- axis represent $\nabla^2\gamma(\vec{0})$ (in red) and the energy of the pulse (in purple) in a.u., respectively. (a) Intensity, $\epsilon = 0.25$ a.u. and (b) Intensity, $\epsilon = 0.75$ a.u.	37

3.5	(a),(b) Geometry of H_3^+ molecule. The black arrows denotes the direction in which the laser is induced. (c) Variation of $\gamma(\vec{0})$ with optical cycle. The x-axis represents the no. of optical cycles and the y1- and y2- axis represent EMD, $\gamma(\vec{0})$ (in red) and the energy of the pulse (in purple) in a.u., respectively. The electric field runs for 12 optical cycles and the pulse is ended after the 6 th optical cycle with polarization along Y-direction with intensity, $\epsilon = 0.25$ a.u., $\omega = 0.21$ a.u., quiver distance, $\alpha_o = 5.668934$ a.u. and the CAP box size is set to 20,26,26 and (d) with polarization along Z-direction with intensity, $\epsilon = 0.75$ a.u., $\omega = 0.21$ a.u., quiver distance, $\alpha_o = 17.007$ a.u. and the CAP box size is set to 20,26,26.	38
3.6	Variation of the laplacian, $\nabla^2\gamma(\vec{0})$, of EMD for H_3^+ , with optical cycle in the presence of a linearly polarized Laser, along (a) Y-direction with $\epsilon = 0.25$ a.u. and (b) along Z-direction with $\epsilon = 0.75$ a.u. The x-axis represents the no. of optical cycles and the y1- and y2- axis represent $\nabla^2\gamma(\vec{0})$ (in red) and the energy of the pulse (in purple) in a.u., respectively.	38
3.7	(a) Geometry of H_2O molecule. The black arrow denotes the direction in which the laser is induced. (b) Variation of $\gamma(\vec{0})$ with optical cycle in the presence of a linearly polarized Laser, along Z-direction. The x-axis represents the no. of optical cycles and the y1- and y2- axis represent EMD, $\gamma(\vec{0})$ (in red) and the energy of the pulse (in purple) in a.u., respectively. The electric field runs for 12 optical cycles and the pulse is ended after the 6 th optical cycle, with intensity, $\epsilon = 0.25$ a.u., $\omega = 0.21$ a.u., quiver distance, $\alpha_o = 5.668934$ a.u., with the CAP box size set to 10,20,20.	39
3.8	Variation of the laplacian, $\nabla^2\gamma(\vec{0})$, of EMD for H_2O , with optical cycle in the presence of a linearly polarized Laser, along Z-direction. The x-axis represents the no. of optical cycles and the y1- and y2- axis represent $\nabla^2\gamma(\vec{0})$ (in red) and the energy of the pulse (in purple) in a.u., respectively and intensity, $\epsilon = 0.25$ a.u.	40

- 3.9 (a) Geometry of C_2H_4 molecule. The black arrow denotes the direction in which the laser is induced. (b) Variation of $\gamma(\vec{0})$ with optical cycle in the presence of a linearly polarized Laser, along Z-direction. The x-axis represents the no. of optical cycles and the y1- and y2- axis represent EMD, $\gamma(\vec{0})$ (in red) and the energy of the pulse (in purple) in a.u., respectively. The electric field runs for 12 optical cycles and the pulse is ended after the 6th optical cycle, with intensity, $\epsilon = 0.25$ a.u., $\omega = 0.21$ a.u., quiver distance, $\alpha_o = 5.668934$ a.u. and (d) with intensity, $\epsilon = 0.75$ a.u., $\omega = 0.21$ a.u., quiver distance, $\alpha_o = 17.007$ a.u., with the CAP box size set to 10,15,20. And, (c) and (e) shows the norms for (b) and (d) respectively. 41
- 3.10 Variation of the laplacian, $\nabla^2\gamma(\vec{0})$, of EMD for C_2H_4 , with optical cycle in the presence of a linearly polarized Laser, along Z-direction with intensities (a) 0.25 a.u. and (b) 0.75 a.u. The x-axis represents the no. of optical cycles and the y1- and y2- axis represent $\nabla^2\gamma(\vec{0})$ (in red) and the energy of the pulse (in purple) in a.u., respectively. 41
- 3.11 (a) Geometry of C_2H_4 molecule. The black arrow denotes the direction in which the laser is induced. (b) Variation of $\gamma(\vec{0})$ with optical cycle in the presence of a linearly polarized Laser, along Z-direction. The x-axis represents the no. of optical cycles and the y1- and y2- axis represent EMD, $\gamma(\vec{0})$ (in red) and the energy of the pulse (in purple) in a.u., respectively. The electric field runs for 12 optical cycles and the pulse is ended after the 6th optical cycle, with intensity, $\epsilon = 0.25$ a.u., $\omega = 0.21$ a.u., quiver distance, $\alpha_o = 5.668934$ a.u. with the CAP box size set to 10,15,20. (c) Norm versus optical cycle. 42
- 3.12 Variation of the laplacian, $\nabla^2\gamma(\vec{0})$, of EMD for C_2H_4 , with optical cycle in the presence of a linearly polarized Laser, along Y-direction with intensity 0.75 a.u. The x-axis represents the no. of optical cycles and the y1- and y2- axis represent $\nabla^2\gamma(\vec{0})$ (in red) and the energy of the pulse (in purple) in a.u., respectively. 42

Atomic Units

symbol	Quantity	Value in a.u	value in S.I.
\hbar	reduced planck constant	1	$1.055 \times 10^{-34} Js$
m_e	electron mass	1	$9.11 \times 10^{-31} kg$
e	electron charge	1	$1.602 \times 10^{-19} C$
a_0	Bohr radius	1	$5.292 \times 10^{-11} m^*$
E_H	Hartree(Energy)	1	$4.360 \times 10^{-18} J^*$
c	speed of light	137.036	$2.998 \times 10^8 m/s$
v_0	velocity	1	$2.18 \times 10^{18} cm/s$
ν_0	frequency	1	$4.13 \times 10^{16} s^{-1}$
ω	Angular frequency	2π	$1.51976 \times 10^{-16} rad/s$
E_0	Electric Field	1	$5.14 \times 10^{11} V/m$
ϵ	Electric Field Intensity	1	$3.509 \times 10^{16} W/cm^2$

* Other important units:

$$a_0 = 0.529 \text{ \AA}$$

$$E_H = 27.21 \text{ eV}$$

Abbreviations

a.u.	Atomic Units
CW	Continuous Wave
EMD	Electron Momentum Density
ED	Electron Density
MESP	Molecular Electrostatic Potential
CP	Critical Point
FT	Fourier Transformation
MO	Molecular Orbital
VBT	Valence Bond Theory
VMD	Visual Molecular Dynamics
HF	Hartree-Fock
CI	Configuration Interaction
CAP	Complex Absorbing Potential

Abstract

Scalar fields are useful for gaining knowledge of the features of any chemical system. Electron momentum density (EMD) is a scalar field, which brings out chemical concepts from the momentum-space point of view. The topography of EMD has been extensively studied and analyzed. One important characteristic of the molecular EMDs is the bond-directionality principle, which states that the maximal nature of the EMD is perpendicular to the position space bonding directions. This allows us to relate, interpret and understand phenomena such as bonding and ionization via molecular properties in the momentum space. This may bear applications for, and better understanding of laser-induced bond-forming and bond-breaking in molecules.

Introduction

Quantum chemistry is a branch of theoretical chemistry that uses physical and mathematical methods to understand the electronic structure of any molecule. Any molecule is made up of positively charged nuclei and negatively charged electrons. Different combinations and arrangements of nuclei and number of electrons in space form different molecules.

To solve a quantum chemical problem, one needs to solve the eigen-value problem.

$$\hat{H}\psi(\mathbf{r}) = E\psi(\mathbf{r}) \quad (1.1)$$

Where \hat{H} is Hamiltonian operator for a system of nuclei and electrons and is independent of time, ψ is the wave function and E is the total energy.

1.1 Time-Independent Schrodinger Equation

For an unperturbed (field-free) system, we use the **Time-Independent Schrödinger equation** to arrive at the wave function and energies for the electrons and nuclei of that system. For every time-independent Hamiltonian operator, \hat{H} , there exists a set of quantum states, ψ_n , known as energy eigenstates, and corresponding real number E_n satisfying the eigenvalue equation:

$$\left[\frac{-\hbar^2}{2m} \nabla^2 + V(\mathbf{r}) \right] \Psi(\mathbf{r}) = E\Psi(\mathbf{r}) \quad (1.2)$$

The only systems that could be calculated exactly by using analytical techniques are those with one electron, such as H-atom, H_2^+ , et. Therefore, different approximations are used to find solutions for a quantum many-body system (e.g. ab-initio methods). One such approximation is the Hartree-Fock approximation [1], which is the most widely used ab-initio calculation. The general Hartree-Fock (HF) method is a quantum mechanical method for electronic structure calculations that uses a single determinantal wave function with no restrictions on the one electron orbitals other than orthonormality and the use of a specific basis set [3]. Since the HF method yields a zeroth order approximation to the exact wavefunction and allows enormous

conceptual simplification due to independent particle interpretation [4], it is one of the most widely used computational method.

1.2 Light matter interaction

Light-Matter interactions result due to interaction between an oscillating electromagnetic (EM) field with a charged entity. Light fields act upon a system to couple their energy states [2],[5]. There are three different approaches to explain the phenomena arising due to light-matter interaction:

1. **Classical Approach:** In this approach, both, matter and light are treated classically, which means that light is treated as an electromagnetic wave [5] and therefore, follows the Maxwell's equation:

$$\frac{\partial}{\partial t} \mathbf{H}(\vec{r}, t) = -\frac{1}{\mu_0} \nabla \times \mathbf{E}(\vec{r}, t) \quad (1.3)$$

Where, $\mathbf{H} = \frac{\mathbf{B}}{\mu_0}$, \mathbf{B} is the magnetic field and \mathbf{E} is the electric field. In this approach, only Maxwell's equation are used (no use of Schrödinger equation) in the time domain. By treating the matter and field classically, one fails to capture any quantum features of the light-matter interactions.

2. **Semi-classical Approach:** In the semi-classical theory, light is treated as an electromagnetic wave and the matter are quantum mechanical objects. These methods are widely used to understand absorption and scattering. Semi-classical approaches can preserve more of the quantum nature of light-matter interactions as compared to the classical approach.
3. **Quantum-mechanical Approach:** In the quantum mechanical approach, light is described in terms of photons for different modes of electromagnetic radiation [5]. Both light and atoms are quantized using field theory. The quantum methods have been developed to understand processes such as spontaneous emission.

In this thesis, a semi-classical approach is followed which is sufficient to understand the behavior of atoms and molecules in the presence of time varying strong fields.

The interaction of an atom with a high-intensity laser field yields a semi-classical model. The electromagnetic field consists of an electric field, $\vec{E}(\vec{r}, t)$ and a magnetic

field, $\vec{B}(\vec{r}, t)$, which can be described from classical scalar and vector potentials, given by Maxwell's equations as follows:

$$\vec{E}(\vec{r}, t) = -\nabla\phi(\vec{r}, t) - \frac{\partial}{\partial t}\vec{A}(\vec{r}, t) \quad \vec{B}(\vec{r}, t) = \nabla \times \vec{A}(\vec{r}, t) \quad (1.4)$$

Here $\vec{A}(\vec{r}, t)$ and $\phi(\vec{r}, t)$ are the vector and scalar potentials, respectively. The dynamics of a system subjected to an external field is described by the **Time-Dependent Schrödinger equation (TDSE)**:

$$i\hbar \frac{\partial \Psi}{\partial t} = \hat{H} \Psi \quad (1.5)$$

The Hamiltonian consists of two parts, the unperturbed Hamiltonian H_0 which consists of the kinetic and potential energy of the system and the time-dependent Hamiltonian $H'(\vec{r}, t)$ of the form $e\phi(\vec{r}, t)$, where e is the electric field component of the electromagnetic field [6][7]. Thus the Hamiltonian can be written as:

$$\hat{H} = \frac{1}{2m_e} [\vec{p} - \frac{e}{c}\vec{A}(\vec{r}, t)]^2 + e\phi + V(\vec{r}) \quad (1.6)$$

1.2.1 Dipole Approximation

The wavelength, λ , of an electromagnetic radiation ($\sim 100\text{nm}$) is generally larger than the size of an atom (0.1 - 0.5 nm). The spatial dependence of the field can, therefore, be ignored [8]. Hence, the expansion of the electric field as Taylor series can be truncated by ignoring the position dependent terms.

$$\begin{aligned} \vec{A}(\vec{r}, t) &= f(t)(\cos(\vec{k} \cdot \vec{r} - \omega t + \delta)) \\ &\cong \frac{f(t)}{2} [e^{i(\vec{k} \cdot \vec{r} - \omega t + \delta)} + e^{-i(\vec{k} \cdot \vec{r} - \omega t + \delta)}] \\ &\cong \frac{f(t)}{2} [e^{i(\vec{k} \cdot \vec{r})} e^{-i(\omega t - \delta)} + e^{-i(\vec{k} \cdot \vec{r})} e^{-i(-\omega t + \delta)}] \end{aligned} \quad (1.7)$$

On expanding $e^{i\vec{k} \cdot \vec{r}}$

$$e^{i\vec{k} \cdot \vec{r}} = 1 + (i\vec{k} \cdot \vec{r}) + \frac{1}{2}(i\vec{k} \cdot \vec{r})^2 + \dots \quad (1.8)$$

With only the first two terms, the vector potential modifies as

$$\begin{aligned} \vec{A}(\vec{r}, t) &\longrightarrow \frac{1}{2}f(t)[(1 + i\vec{k} \cdot \vec{r})e^{i(\omega t - \delta)} + (1 - i\vec{k} \cdot \vec{r})e^{-i(\omega t - \delta)}]\hat{e}_z \\ &\cong f(t)[\cos(\omega t - \delta) + \vec{k} \cdot \vec{r}] \\ &\cong \vec{A}^0(t) + \vec{A}^1(r, t) \end{aligned} \quad (1.9)$$

Here, $\vec{A}_0(t)$ is the vector potential within dipole approximation. The $\vec{k} \cdot \vec{r}$ term vanishes and $\vec{A}^1(r, t)$ is only a correction term. Since the vector potential is independent of \vec{r} with implications of spatial homogeneity, the magnetic field, $\vec{B} = 0$. The time dependent vector potential term thus finally assumes the form

$$\vec{A}^0(t) = f(t) \cdot \cos(\omega t + \phi) \epsilon_z \hat{z} \quad (1.10)$$

This spatially independent but time dependent potential adds up to the overall Hamiltonian in addition to the innate free field Hamiltonian. For a CW laser, $f(t) = 1$ and thus the TDSE for the system can be finally written as:

$$i\hbar \frac{\partial \psi(\vec{r}, t)}{\partial t} = \left[-\frac{\hbar^2}{2m_e} \nabla^2 + \epsilon_z \cdot \vec{r} \cos(\omega t) + V(\vec{r}) \right] \psi(\vec{r}, t) \quad (1.11)$$

1.3 Electric Fields

1.3.1 Linear Homogeneous Electric Field

In a linear homogeneous electric field atoms are in constant, background electric fields. These fields break various symmetries of the problem, we expect to see a splitting in the degeneracies of states. If we take an electric field in the z-direction ($E = E_0 \hat{z}$), the Hamiltonian for an H_2 molecule then becomes:

$$\hat{H} = -\frac{\hbar^2}{2m} \nabla^2 - \frac{e^2}{4\pi\epsilon_0 r} + eE_0 \hat{z} \quad (1.12)$$

The potential energy, $V(\hat{z}) = eE_0 \hat{z} - \frac{e^2}{4\pi\epsilon_0 r}$, is plotted w.r.t. the z-axis: The potential

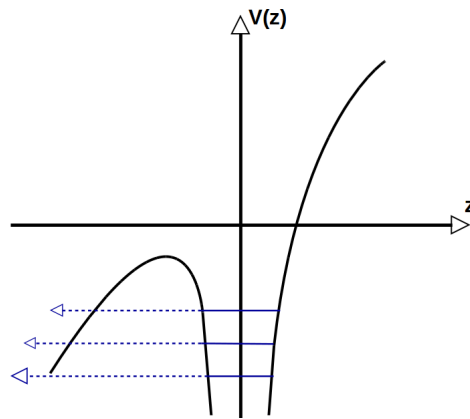


Fig. 1.1: Potential energy curve for a system that is being subjected to a static electric field in Z-direction

is unbounded below as $z \rightarrow \infty$. This means that all electron bound states, with wavefunctions localised near the origin, are now unstable. Any electron can tunnel through the barrier to the left, and then be accelerated by the electric field to $z \rightarrow \infty$.

1.3.2 Polarized Laser Pulse

Polarization is the process of restricting the direction of the oscillations of light using a polarizer. An unpolarized electric field oscillates randomly in all directions. A linearly polarized field along the x-direction will be of the form:

$$\vec{e} = f(t)E_o\cos(\omega t)\hat{x} \quad (1.13)$$

where, $f(t)$ is an envelope provide over the pulse. Fig.(1.2) shows how a linearly polarized field in the presence of a sine squared envelope looks like.

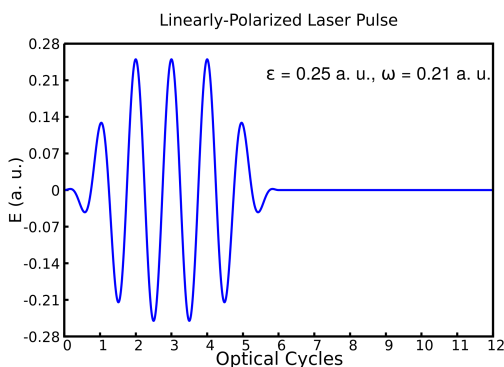


Fig. 1.2: Linearly polarised electric field with a sine squared envelope over it

Having laid the background for Quantum mechanics and Light matter interaction, we shall now move to **Molecular electron momentum densities**, which is an important tool of chemistry. Like electron density, the momentum density is also a **Scalar field**.

1.4 Scalar Fields

A scalar field is a function that gives us a single value of some variable for every point in space. The scalar may either be a (dimensionless) mathematical number or a physical quantity. The interpretative strength of scalar fields is very useful for

studies in interpretative chemistry.

Scalar fields such as molecular electron density (MED), molecular electrostatic potential (MESP), molecular electron momentum density (EMD) etc. are more closer to the heart of experimental science and they have a direct connection with scattering experiments in general. In this thesis we will primarily focus on electron momentum densities (EMDs). Before getting to EMDs in detail, we will have to first look at electron density (ED) and understand how are EMD and ED related.

1.4.1 Electron density

Electron density is the measure of the probability of finding an electron at an infinitesimal element of space surrounding any given point.

For an N -electron M -atom molecule within Born-Oppenheimer approximation, the Hamiltonian operator, \hat{H} (in a.u.), is given by the equation:

$$\hat{H} = -\sum_{i=1}^N \frac{1}{2} \nabla_i^2 - \sum_{i=1}^N \sum_{A=1}^M \frac{Z_A}{|\vec{r}_i - \vec{R}_A|} + \sum_{i=1}^N \sum_{j>1}^N \frac{1}{|\vec{r}_i - \vec{r}_j|} + \sum_{A=1}^M \sum_{B>1}^M \frac{Z_A Z_B}{|\vec{R}_A - \vec{R}_B|} \quad (1.14)$$

The nuclei with charges Z_A are at position vectors \vec{R}_A and the electrons at position vectors \vec{r}_i . The electronic charge density is derived from an N -electron wavefunction ψ via:

$$\rho(\vec{r}) = N \int \psi^*(\vec{r}, \vec{r}_2, \dots, \vec{r}_N) \psi(\vec{r}, \vec{r}_2, \dots, \vec{r}_N) d\vec{r}_2 \dots d\vec{r}_N \quad (1.15)$$

The electron density $\rho(\vec{r})$ is the fundamental property that characterises the ground state of the system. The energy of a system can be uniquely defined, once $\rho(\vec{r})$ is known, and from there a diverse range of molecular properties can be deduced. The electron density has an experimental realization in coherent X-ray scattering experiments.

However, the molecular properties deduced from $\rho(\vec{r})$ are only limited to the position space. Since, molecules possess kinetic energy, further information about the nature of the electrons and the properties of their distribution could be provided by a function which is a measure of the number of electrons moving in an infinitesimal velocity range. For that we will have to look into the momentum space.

1.4.2 Relationship between the position space and momentum space

To understand the relationship between the position and momentum, we look at a simple pendulum.

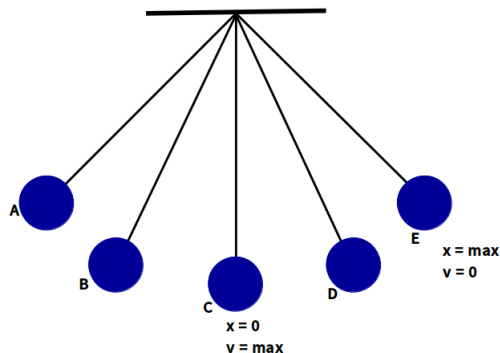


Fig. 1.3: Motion of a pendulum

In Fig.(1.3), we see that at C, when displacement is zero, velocity is maximum, which implies maximum momentum at C. At E, when displacement is maximum, velocity is zero, which implies zero momenta. Hence, position and momentum are complimentary quantities and therefore, if a function is given in position space, $f(\vec{r})$, then its Fourier transform obtains the function in momentum space, $f(\vec{p})$. The momentum space wavefunction can therefore, be obtained via a 3N-dimensional Fourier transformation of the corresponding position space wavefunction[9].

$$\Phi(\vec{p}) = (2\pi)^{-\frac{3N}{2}} \int \Psi(\vec{r}_1, \vec{r}_2, \dots, \vec{r}_N) e^{-i \sum_i \vec{p}_i \cdot \vec{r}_i} d\vec{r}_1 d\vec{r}_2 \dots d\vec{r}_N \quad (1.16)$$

This transformation preserves directions, thus it is still correct in momentum space to talk about directions perpendicular to the plane of a planar molecule as well as reflection in a symmetry plane or rotation about a symmetry axis of a molecule and of directions parallel to certain bonds [10]. However, in the momentum space information about the origin is lost.

1.4.3 Electron Momentum Density

The electron momentum density is a measure of the number of electrons moving with a given velocity in a given volume defined in the momentum space. It can be extracted from the momentum space wave function as follows [10]

$$\gamma(\vec{p}) = N \sum_{spins} \int \phi^*(\vec{p}, \vec{p}_2, \dots, \vec{p}_N) \phi(\vec{p}, \vec{p}_2, \dots, \vec{p}_N) d\vec{p}_2 \dots d\vec{p}_N \quad (1.17)$$

According to the inverse weighting of the Fourier transform relation, the electron momentum distributions turns out to be more informative in the low momentum (large r) region [11]. Thus, its more favourable to use EMDs for studying the valence electron behaviour. Electron momentum densities are experimentally accessible via techniques such as Compton scattering, positron annihilation followed by angular correlation etc.

For a better understanding of molecular structures, topographies of the ground-state EMDs are studied and analyzed for critical points (CPs), especially, the ones at $|\vec{p}| = 0$. Initially, topographical studies of atomic and molecular scalar fields concentrated on securing a systematic understanding of the nature of the function and to use that knowledge for an interpretative purpose.

1.5 Experimental measures of EMD

1.5.1 Compton Scattering

Compton scattering is an inelastic scattering that probes momentum distributions of electrons in condensed matter. It occurs due to interaction of a photon with the free electrons of a system. EMDs are closely related to intensities obtained from Compton scattering experiments. When monochromatic photons are Compton scattered (inelastically scattered) in a fixed direction, the observed energy spectrum of the scattered photons is Doppler-broadened due to the motion of the target electrons.

The shift in the wavelength of the photon after being scattered is given by:

$$\lambda' - \lambda = \frac{h}{m_e c} (1 - \cos\theta) \quad (1.18)$$

The Compton profile is related to the spherically averaged electron momentum density [12] [13], $\gamma(\vec{p})$ via the relation:

$$J(p_z) = 2\pi \int_{|p_z|}^{\infty} \gamma(p) p dp \quad (1.19)$$

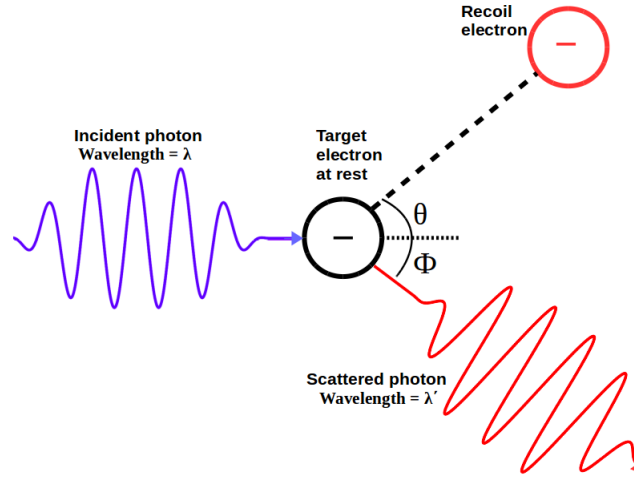


Fig. 1.4: A schematic diagram of Compton scattering. An incident photon of wavelength λ collides with an electron at rest. A new scattered photon of wavelength λ' emerges at an angle Φ and the electron recoils by an angle θ

Reciprocally,

$$\gamma(p) = \frac{-1}{2\pi} p^{-1} \frac{dJ(p_z)}{dp_z} \quad (1.20)$$

The study and measurements of Compton profiles have received a good deal of attention in the past decade. The reason for such an interest is that with the advent of intense γ -ray and synchrotron radiation sources very accurate determination of the momentum space properties of electrons in the sample has become possible.

1.5.2 Positron Annihilation Experiment

Positrons are anti-particle counterpart of electrons, created by beta decay or pair production. Positrons and electrons are complementary states of matter, and upon interaction a positron can easily annihilate an electron, and their kinetic and rest mass energies are dissipated as the energy of two gamma-rays, in exactly opposite directions. Information about the behaviour of electrons, that are annihilated by positrons, is then obtained by measuring various properties of the subsequent annihilation quanta [14][15].

There are different categories of annihilation experiments to obtain information about electrons. To access the electron momentum densities via positron annihilation, two-photon angular correlation experiments are used [15]. The two-photon angular correlation depends on the momentum of the positron-electron pair.

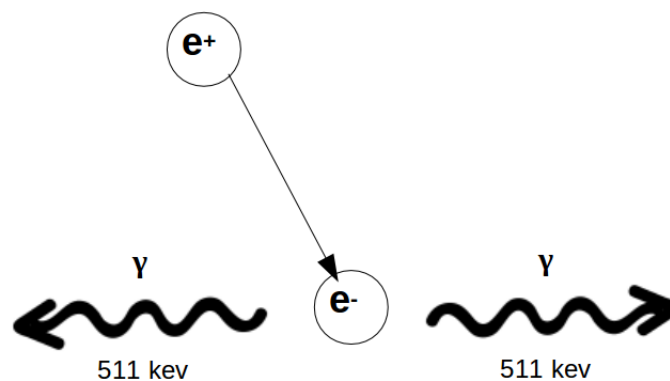


Fig. 1.5: Schematic for positron annihilation of an electron.

1.6 Bond-directionality Principle

An important characteristic of the molecular EMDs is the **bond-directionality principle**, which states that the maximal nature of the EMD is perpendicular to the position space bonding directions. Being connected by an FT, the wavefunctions in position and momentum spaces bear a reciprocal relation to each other, hence a narrow wave function in position space leads to a broad one in momentum space and vice versa [16].

The Molecular orbital wavefunction of H_2 in position space, can be written as:

$$\Psi_{MO}(\vec{r}_1) = \frac{1}{\sqrt{2(1+S^2)}} [\psi_A(\vec{r}_1) + \psi_B(\vec{r}_1)] \quad (1.21)$$

Where, $\psi_A(\vec{r}_1)$ and $\psi_B(\vec{r}_1)$ is the 1s atomic Slater function with the atoms being centred at position vectors \vec{R}_A and \vec{R}_B respectively. The overlap between these functions is given by S . Fourier transforming eqn.(1.21) and integrating over momentum coordinates of one particle, we get the EMD distribution of H_2 molecule, which is as follows:

$$\gamma(\vec{p}) = \frac{1 + \cos[\vec{p} \cdot (\vec{R}_A - \vec{R}_B)]}{1 + S^2} |A(\vec{p})|^2 \quad (1.22)$$

Here $(\vec{R}_A - \vec{R}_B)$ denotes the bonding vector and $A(\vec{p})$ is the Fourier transform of the 1s atomic Slater function. The cos term, diffraction factor, in eqn.(1.22) induces maximality in a momentum direction perpendicular to bonding direction, known as **Coulson's bond directionality principle** and also induces oscillations which is termed as the **bond oscillation principle**. This interpretation allows us to relate and effect chemical phenomena like bonding and ionization in the momentum space.

1.7 Thesis Outline

The idea of this thesis is to look at the bond directionality and bond oscillation principles in the above discussed molecular systems in the absence of field and later observe the changes in the same in presence of an external oscillating electric field. The 2nd chapter discusses the tools of topography and the important characteristics of EMD like the bond-directionality principle, important for our study, in more detail. The 3rd and 4th chapter includes the study of bond-directionality principle in different molecular systems in great detail and their EMDs in absence and presence of an external oscillating electric field and the results and interpretations that we could arrive at from our study.

References

- [1] A. Szabo, N. S. Ostlund, *Modern Quantum Chemistry: Introduction to Advanced Electronic Structure Theory*, McGraw-Hill, Rhode Island, (1989).
- [2] P. F. Bernath, *Spectra of Atoms and Molecules*, Oxford University press, Third Edition.
- [3] S. H. Schiffer, H. C. Andersen, *J. Chem. Phys.*, **99**, 1901-1913 (1993).
- [4] W. A. Goddard, *Phys. Rev.* **157**, 81-93 (1967).
- [5] P. Vasa, *Strong light-matter interaction*.
- [6] R. M. A. Vivirito, P.L. Knight, *J. Phys. B. At. Mol. Opt. Phys.*, **28**, 4357-4375 (1995).
- [7] F. Morales, M. Richter, S. Patchkovskii, O. Smirnova, *Proc Natl Acad Sci U S A* , **108**, 16906–16911 (2011).
- [8] N. H. List, J. Kauczor, T. Saue, H. J. A. Jensen, P. Norman, *J. Chem. Phys.*, **142**, 244111 (2015).
- [9] D. C. Rawlings, E. R. Davidson, *J. Chem. Phys.*, **89**, 969-974 (1985).
- [10] U. Roy, S. Ghosh, T. Shreecharan, K. Bhattacharya, *Rev. Mex. Fis. E*, **54**, 160-168 (2008).
- [11] M. Defranceschi, G. Berthier, *J. Phys. France*, **51**, 2791-2800 (1990).
- [12] M. J. Cooper, *Adv.Phys.*, **20**, 453-491 (1971).
- [13] A. C. Tanner, I. R. Epstein, *J. Chem. Phys.*, **61**, 4251 (1974).
- [14] C. F. Coleman, *NDT International*, **10**, 227-234 (1977).
- [15] S. Berko and J. Mader, *Appl. Phys.*, **5**, 287-306 (1975).
- [16] C. A. Coulson, *Math. Proc. Cam. Phil. Soc.*, **37**, 55-66 (1941).
- [17] S. A. Kulkarni, S. R. Gadre, *Chem. Phys. Lett.*, **274**, 255-263 (1997).
- [18] A. J. Thakkar, *J. Chem. Phys.*, **76**, 746 (1982).

[19] S. Gadre, R. N. Shirsat, *Electrostatics of Atoms and Molecules* (2001).

Bond directionality in Electron Momentum Densities of Field-free Molecules

The following chapter discusses, the bond-directionality principle in different chemical systems, such as the Dihydrogen molecule (H_2), Trihydrogen cation (H_3^+), water (H_2O) and ethylene (C_2H_4) in the absence of an electric field. We have tried to look at the variation in EMD with changing bond length for H_2 and H_3^+ , to look at the oscillations that set in with increasing bond length. The last section of this chapter discusses pair-wise electron momentum densities and how they are important for polyatomic systems.

2.1 Dihydrogen (H_2)

We try to arrive at an expression for the bond-directionality principle using the MO and Valence bond approximation.

2.1.1 Bond Directionality Principle : MO and VBT approximation

- **MO approximation:**

For H_2 , consider the molecular orbital for an electron forming part of a bond between nuclei H_A and H_B :

$$\Psi_{MO}(\vec{r}) = \frac{1}{\sqrt{2(1+S^2)}} [\psi_A(\vec{r}) + \psi_B(\vec{r})] \quad (2.1)$$

Where, $\psi_A(\vec{r})$ and $\psi_B(\vec{r})$ is the 1s atomic Slater function with the atoms being centred at position vectors \vec{R}_A and \vec{R}_B respectively, given as:

$$\psi_A(\vec{r}) = \left(\frac{\alpha^3}{\pi} \right)^{\frac{1}{2}} e^{-\alpha|\vec{r}-\vec{R}_\text{A}|} \quad (2.2)$$

and, S is the overlap between two slater functions. The Fourier transformation of eqn (2.20) will give us the wavefunction in momentum space.

$$\phi_A(\vec{p}) = \left(\frac{2\alpha}{\pi}\right)^{1/2} \frac{8\pi\alpha^{5/2}}{(\alpha^2 + p^2)^2} e^{-i\vec{p}\cdot\vec{R}_A} \quad (2.3)$$

$$\Phi(\vec{p}) = \frac{1}{\sqrt{2(1+S^2)}} [e^{-i\vec{p}\cdot\vec{R}_A} + e^{-i\vec{p}\cdot\vec{R}_B}] A(\vec{p}) \quad (2.4)$$

Momentum density can be given as:

$$\begin{aligned} \gamma(\vec{p}) &= |\Phi(\vec{p})|^2 = \Phi(\vec{p})\Phi^*(\vec{p}) \\ &= \frac{1}{2(1+S^2)} [e^{-i\vec{p}\cdot\vec{R}_A} + e^{-i\vec{p}\cdot\vec{R}_B}] [e^{i\vec{p}\cdot\vec{R}_A} + e^{i\vec{p}\cdot\vec{R}_B}] A(\vec{p}) A^*(\vec{p}) \\ &= \frac{1}{2(1+S^2)} [2 + e^{-i\vec{p}\cdot\vec{R}_A} e^{-i\vec{p}\cdot\vec{R}_B} + e^{-i\vec{p}\cdot\vec{R}_A} e^{-i\vec{p}\cdot\vec{R}_B}] |A(\vec{p})|^2 \\ &= \frac{1}{2(1+S^2)} [2 + e^{-i\vec{p}\cdot(\vec{R}_A - \vec{R}_B)} + e^{i\vec{p}\cdot(\vec{R}_A - \vec{R}_B)}] |A(\vec{p})|^2 \\ &= \frac{1}{1+S^2} \left[1 + \frac{e^{-i\vec{p}\cdot(\vec{R}_A - \vec{R}_B)} + e^{i\vec{p}\cdot(\vec{R}_A - \vec{R}_B)}}{2}\right] |A(\vec{p})|^2 \\ &= \frac{1 + \cos \vec{p}\cdot(\vec{R}_A - \vec{R}_B)}{1+S^2} |A(\vec{p})|^2 \end{aligned} \quad (2.5)$$

Here $(\vec{R}_A - \vec{R}_B)$ denotes the bonding vector and $A(\vec{p})$ is the Fourier transform of the 1s atomic slater function.

- **VB approximation:**

The Valence bond orbital wavefunction for H_2 :

$$\Psi_{VB}(\vec{r}_1, \vec{r}_2) = \frac{1}{\sqrt{2(1+S)}} [\psi_A(\vec{r}_1)\psi_B(\vec{r}_2) + \psi_A(\vec{r}_2)\psi_B(\vec{r}_1)] \quad (2.6)$$

Then wavefunction in momentum space can be given as:

$$\phi(\vec{p}_1, \vec{p}_2) = \frac{1}{\sqrt{2(1+S)}} [e^{-i(\vec{p}_1\cdot\vec{R}_A + \vec{p}_2\cdot\vec{R}_B)} + e^{-i(\vec{p}_2\cdot\vec{R}_A + \vec{p}_1\cdot\vec{R}_B)}] A(\vec{p}_1) A(\vec{p}_2) \quad (2.7)$$

Momentum density will then be:

$$\begin{aligned} \gamma(\vec{p}) &= |\Phi(\vec{p}_1, \vec{p}_2)|^2 = \Phi(\vec{p})\Phi^*(\vec{p}) \\ &= \frac{1}{2(1+S)} [e^{-i(\vec{p}_1\cdot\vec{R}_A + \vec{p}_2\cdot\vec{R}_B)} + e^{-i(\vec{p}_2\cdot\vec{R}_A + \vec{p}_1\cdot\vec{R}_B)}] \\ &\quad [e^{i(\vec{p}_1\cdot\vec{R}_A + \vec{p}_2\cdot\vec{R}_B)} + e^{i(\vec{p}_2\cdot\vec{R}_A + \vec{p}_1\cdot\vec{R}_B)}] |A(\vec{p}_1)|^2 |A(\vec{p}_2)|^2 \end{aligned}$$

$$\begin{aligned}
\gamma(\vec{p}) &= \frac{1}{2(1+S)} [2 + e^{-i(\vec{p}_1 - \vec{p}_2) \cdot (\vec{R}_A - \vec{R}_B)} + e^{i(\vec{p}_1 - \vec{p}_2) \cdot (\vec{R}_A - \vec{R}_B)}] |A(\vec{p}_1)|^2 |A(\vec{p}_2)|^2 \\
&= \frac{1}{2(1+S)} [2 + 2 \cos(\vec{p}_1 - \vec{p}_2) \cdot (\vec{R}_A - \vec{R}_B)] |A(\vec{p}_1)|^2 |A(\vec{p}_2)|^2 \\
&= \frac{1 + \cos(\vec{p}_1 - \vec{p}_2) \cdot (\vec{R}_A - \vec{R}_B)}{1+S} |A(\vec{p}_1)|^2 |A(\vec{p}_2)|^2
\end{aligned}$$

The momentum density corresponding to electron 1 can then be obtained by integrating the above equation over \vec{p}_2 as follows:

$$|\Phi(\vec{p}_1)|^2 = \frac{1 + \cos \vec{p}_1 \cdot (\vec{R}_A - \vec{R}_B)}{1+S} |A(\vec{p}_1)|^2 \quad (2.8)$$

For the momentum density to be maximum, the diffraction term, *i.e.* the cos term in eqn.(2.5) and eqn.(2.8), should be equal to 1. So,

$$\begin{aligned}
\cos \vec{p} \cdot (\vec{R}_A - \vec{R}_B) &= 1 \\
\implies \vec{p} \cdot (\vec{R}_A - \vec{R}_B) &= 0 \\
\implies |\vec{p}| |\vec{R}_A - \vec{R}_B| \cos \theta &= 0 \\
\implies \theta &= 90^\circ
\end{aligned}$$

Thus the EMD is maximal in a direction perpendicular to the position space bonding direction ($\vec{R}_A - \vec{R}_B$).

We would also like to look at the consequences of increasing the bond length, *i.e.* increasing $|\vec{R}_A - \vec{R}_B|$. Looking at eqn.(2.5), it can be said that upon increasing the bond-length, we could see greater oscillations because each atom would have its own sepaarate oscillations, which would increase as the separation between two atoms increase.

2.1.2 Variation of EMD with increasing bond length

We varied the H-H bond length from 0.05 a.u. to 25 a.u. and calculated the EMDs at each bond length using the restricted Hartree-Fock (RHF) and full configuration interaction (CI) method methods. In the RHF method H_2 dissociates as H^+ and H^- , while in the CI method it dissociates as 2 H atoms, which is what we want. Hence we've used both RHF and full CI method for comparision. The *coemd-ref* basis set for the S, P and D shells with their numbers modified by an even-tempered extrapolation of the basis has been used in the following calculations.

Fig.(2.1) shows the potential energy curve for the ground state of the H_2 molecule calculate using the full CI method at each H-H bond length. The EMD and Laplacian at each of the shown bond length was calculated. Fig.2.2(a) shows the variation of

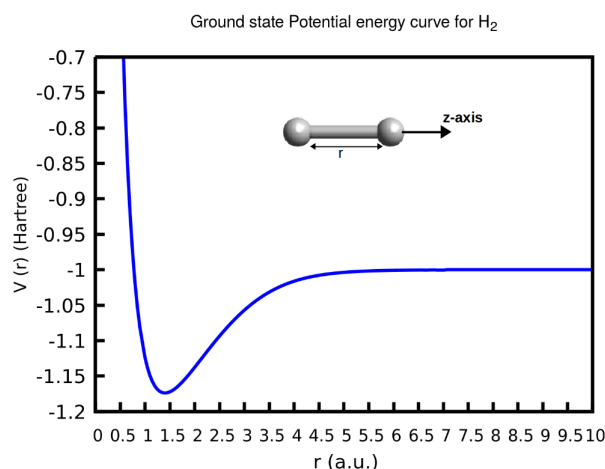


Fig. 2.1: Ground state potential energy curve for H_2 , calculated using the full CI method with extended coemd-ref basis set.

EMD at $|\vec{p}| = 0$ with increasing bond length. We can see from the curve for EMD that the value of $\gamma(\vec{0})$ increases with increasing bond-length in case of the RHF method except around $r = 11$ a.u.. We have already seen that the valence character of any system is observed at $|\vec{p}| = 0$. When $r = 0$, the two H atoms are strongly bonded and therefore have a very weak valence character, so the $\gamma(\vec{0})$ value is low at low r . As r increases, the separation of the H atoms lead to an increase in the valence character, thereby increasing $\gamma(\vec{0})$. However, for the full CI method, we see that the EMD first increases, then decreases a little and remains the same thereafter, this may be due to the fact that H_2 dissociates as 2 H atoms. The data from the full-CI method is more believable because of its channel of dissociation.

Fig.2.2(b) shows the variation of the Laplacian of the EMD at $|\vec{p}| = 0$ with increasing bond length. The Laplacian of a function $f(x)$ at x_0 measures how much $f(x_0)$ deviates from average values of f on either side of it. If, at a given point x_0 , the function is the same as the average over surrounding points, then the Laplacian vanishes. On the other hand, if the function is far from that average then the Laplacian is far from zero. From the blue curve (full-CI) of the Laplacian we can see that when the values of $\gamma(\vec{0})$ are increasing, the laplacian is far from zero. This is because the deviation at each point from the average values around that point is high. However, when the $\gamma(\vec{0})$ values start converging, the laplacian gets closer to zero because the deviation is now almost negligible.

Also, the dip in the EMD-red curve around 11 a.u. Laplacian-red curve becoming less negative around the same bond length is indicative of a loss in maximal character at $|\vec{p}| = 0$.

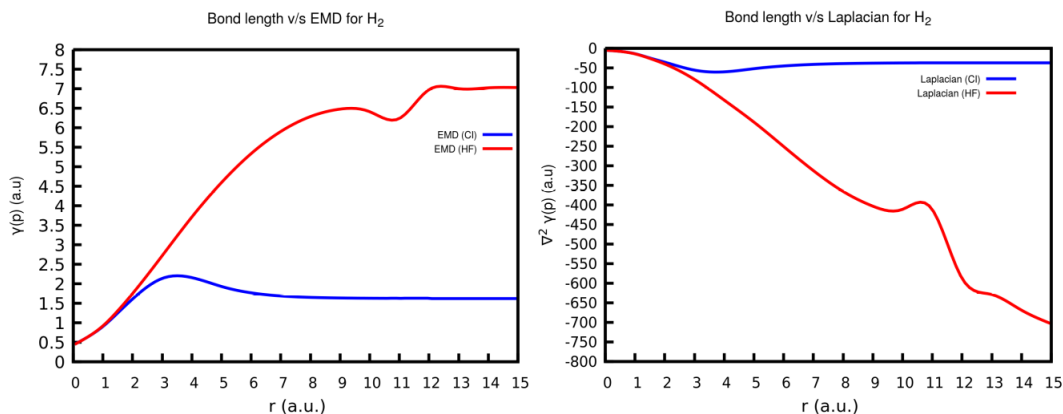
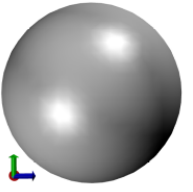
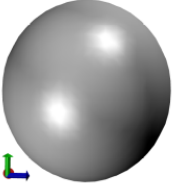
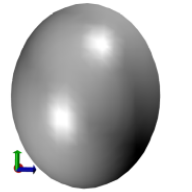
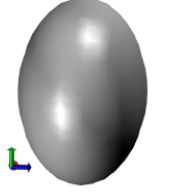
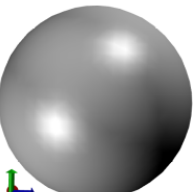
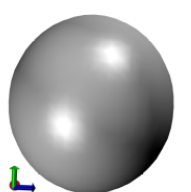
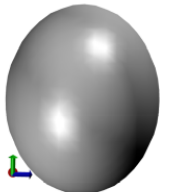
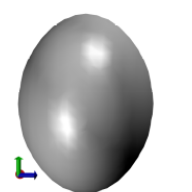


Fig. 2.2: A plot of (a) EMD and (b) Laplacian of EMD for H₂ at $|\vec{p}| = 0$ as a function of the bond length. The values of both EMD and Laplacian at $|\vec{p}| = 0$ was calculated using an in-house code for momentum space properties.

We've also tried plotting the isosurfaces for EMDs at varying bond lengths of 0.05 a.u. to 7 a.u., using both RHF and full CI method and tried comparing the isosurfaces from the two methods.

Bond length(a.u.)	0.05	1.044	2.038	3.032
HF calculations				
Isovalue range	0 - 0.44175	0 - 0.94809	0 - 1.78023	0 - 2.74963
CI Calculations (NSOs)				
Isovalue range	0 - 0.448103	0 - 0.92893	0 - 1.63252	0 - 2.1434


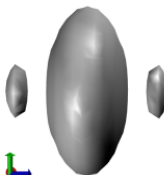
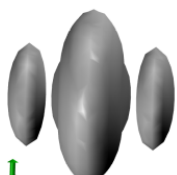
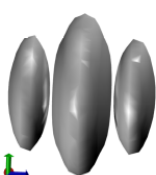
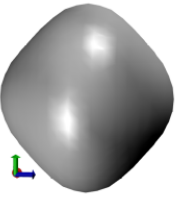
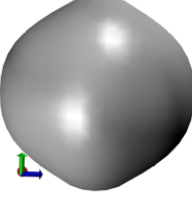
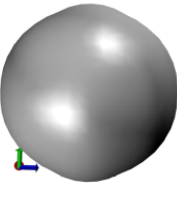
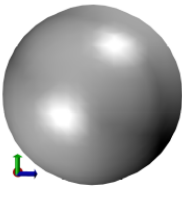
Bond length(a.u.)	4.026	5.021	6.014	7.008
HF calculations				
Isovalue range	0 - 3.73283	0 - 4.61022	0 - 5.34921	0 - 5.9231
CI Calculations (NSOs)				
Isovalue range	0 - 2.15118	0 - 1.93256	0 - 1.76321	0 - 1.68418

Fig. 2.3: Isosurfaces of EMDs for H_2 for varying H-H bond length using the extended coemd-ref basis set, visualized using VMD at an isovalue of 0.05

From fig.(2.3), we can see that when the separation between the two H atoms is small, there are no oscillations and the isosurface also looks equivalent on all axes. As we move closer to the equilibrium bond length (~ 1.4 a.u.), we see that the maximal nature of the EMD is perpendicular to the position space bonding directions. Upon further increase in the H-H bond length we can see that the oscillations start to set in, and the number of oscillations increase upon increase in bond length. This may be because at higher bond lengths, the atoms no longer remain bonded and have individual oscillations, and the number of these oscillations increase as the separation between the two H atoms.

2.2 Trihydrogen cation (H_3^+)

We have chosen Trihydrogen cation (H_3^+) for its geometry, which maybe interesting to analyze in terms of EMDs. It has a D_{3h} symmetry. We have tried to come at an analytical expression for bond-directionality principle for this as well.

2.2.1 Bond Directionality Principle : MO and VBT approximation

- **MO approximation :**

For H_3^+ , we again consider molecular orbital for an electron forming part of a bond between nuclei H_A , H_B and H_C :

$$\Psi_{MO}(\vec{r}) = \frac{1}{\sqrt{2(1+S^2)}}[\psi_A(\vec{r}) + \psi_B(\vec{r}) + \psi_C(\vec{r})] \quad (2.9)$$

The Fourier transformation of eqn (2.9) will give us the wavefunction in momentum space.

$$\Phi(\vec{p}) = \frac{1}{\sqrt{2(1+S^2)}}[e^{-i\vec{p} \cdot \vec{R}_A} + e^{-i\vec{p} \cdot \vec{R}_B} + e^{-i\vec{p} \cdot \vec{R}_C}]A(\vec{p}) \quad (2.10)$$

Momentum density, can then be given as:

$$\begin{aligned} |\Phi(\vec{p})|^2 &= \Phi(\vec{p})\Phi^*(\vec{p}) \\ &= \frac{1}{2(1+S^2)}[e^{-i\vec{p} \cdot \vec{R}_A} + e^{-i\vec{p} \cdot \vec{R}_B} + e^{-i\vec{p} \cdot \vec{R}_C}][e^{i\vec{p} \cdot \vec{R}_A} + e^{i\vec{p} \cdot \vec{R}_B} + e^{i\vec{p} \cdot \vec{R}_C}]A(\vec{p})A^*(\vec{p}) \\ &= \frac{1}{2(1+S^2)}[3 + e^{-i\vec{p} \cdot (\vec{R}_A - \vec{R}_B)} + e^{i\vec{p} \cdot (\vec{R}_A - \vec{R}_B)} + e^{-i\vec{p} \cdot (\vec{R}_A - \vec{R}_C)} + e^{i\vec{p} \cdot (\vec{R}_A - \vec{R}_C)} \\ &\quad + e^{-i\vec{p} \cdot (\vec{R}_B - \vec{R}_C)} + e^{i\vec{p} \cdot (\vec{R}_B - \vec{R}_C)}]|A(\vec{p})|^2 \\ &= \frac{1}{2(1+S^2)}[3 + 2 \cos \vec{p} \cdot (\vec{R}_A - \vec{R}_B) + 2 \cos \vec{p} \cdot (\vec{R}_A - \vec{R}_C) + \\ &\quad 2 \cos \vec{p} \cdot (\vec{R}_B - \vec{R}_C)]|A(\vec{p})|^2 \end{aligned} \quad (2.11)$$

- **VBT approximation :**

The Valence bond orbital wavefunction for H_2 :

$$\begin{aligned} \Psi_{VB}(\vec{r}_1, \vec{r}_2) &= \frac{1}{\sqrt{6(1+S)}}[\psi_A(\vec{r}_1)\psi_B(\vec{r}_2) + \psi_A(\vec{r}_1)\psi_C(\vec{r}_2) + \psi_B(\vec{r}_1)\psi_C(\vec{r}_2) \\ &\quad + \psi_A(\vec{r}_2)\psi_B(\vec{r}_1) + \psi_A(\vec{r}_2)\psi_C(\vec{r}_1) + \psi_B(\vec{r}_2)\psi_C(\vec{r}_1)] \end{aligned}$$

Then wavefunction in momentum space can be given as:

$$\begin{aligned}\phi(\vec{p}_1, \vec{p}_2) = & \frac{1}{\sqrt{6(1+S)}} [e^{-i(\vec{p}_1 \cdot \vec{R}_A + \vec{p}_2 \cdot \vec{R}_B)} + e^{-i(\vec{p}_1 \cdot \vec{R}_A + \vec{p}_2 \cdot \vec{R}_C)} + \\ & e^{-i(\vec{p}_1 \cdot \vec{R}_B + \vec{p}_2 \cdot \vec{R}_C)} + e^{-i(\vec{p}_1 \cdot \vec{R}_B + \vec{p}_2 \cdot \vec{R}_A)} \\ & + e^{-i(\vec{p}_1 \cdot \vec{R}_C + \vec{p}_2 \cdot \vec{R}_A)} + e^{-i(\vec{p}_1 \cdot \vec{R}_C + \vec{p}_2 \cdot \vec{R}_B)}] A(\vec{p}_1) A(\vec{p}_2)\end{aligned}$$

Momentum density will then be:

$$\begin{aligned}|\Phi(\vec{p}_1, \vec{p}_2)|^2 = & \Phi(\vec{p}) \Phi^*(\vec{p}) \\ = & \frac{1}{6(1+S)} [6 + 2 \cos \vec{p}_2 \cdot (\vec{R}_B - \vec{R}_C) + 2 \cos[\vec{p}_1 \cdot (\vec{R}_A - \vec{R}_B) + \vec{p}_2 \cdot (\vec{R}_B - \vec{R}_C)] \\ & + 2 \cos(\vec{p}_1 - \vec{p}_2) \cdot (\vec{R}_A - \vec{R}_B) + 2 \cos[\vec{p}_1 \cdot (\vec{R}_A - \vec{R}_C) + \vec{p}_2 \cdot (\vec{R}_B - \vec{R}_A)] \\ & + 2 \cos \vec{p}_1 \cdot (\vec{R}_A - \vec{R}_C) + 2 \cos \vec{p}_1 \cdot (\vec{R}_A - \vec{R}_B) \\ & + 2 \cos[\vec{p}_1 \cdot (\vec{R}_A - \vec{R}_B) + \vec{p}_2 \cdot (\vec{R}_C - \vec{R}_A)] \\ & + 2 \cos(\vec{p}_1 - \vec{p}_2) \cdot (\vec{R}_A - \vec{R}_C) + 2 \cos[\vec{p}_1 \cdot (\vec{R}_A - \vec{R}_C) + \vec{p}_2 \cdot (\vec{R}_C - \vec{R}_B)] \\ & + 2 \cos \vec{p}_2 \cdot (\vec{R}_C - \vec{R}_A) + 2 \cos[\vec{p}_1 \cdot (\vec{R}_B - \vec{R}_C) + \vec{p}_2 \cdot (\vec{R}_C - \vec{R}_A)] \\ & + 2 \cos(\vec{p}_1 - \vec{p}_2) \cdot (\vec{R}_B - \vec{R}_C) \\ & + 2 \cos \vec{p}_1 \cdot (\vec{R}_B - \vec{R}_C) + 2 \cos[\vec{p}_1 \cdot (\vec{R}_B - \vec{R}_C) + \vec{p}_2 \cdot (\vec{R}_A - \vec{R}_B)] \\ & + 2 \cos \vec{p}_2 \cdot (\vec{R}_A - \vec{R}_B)] |A(\vec{p}_1)|^2 |A(\vec{p}_2)|^2\end{aligned}$$

The momentum density corresponding to electron 1 can then be obtained by integrating the above equation over \vec{p}_2 .

$$\begin{aligned}|\Phi(\vec{p}_1)|^2 = & \frac{1}{6(1+S)} [6 + 8 \cos \vec{p}_1 \cdot (\vec{R}_A - \vec{R}_B) + 8 \cos \vec{p}_1 \cdot (\vec{R}_A - \vec{R}_C) + \\ & 8 \cos \vec{p}_1 \cdot (\vec{R}_B - \vec{R}_C)] |A(\vec{p}_1)|^2\end{aligned}\quad (2.12)$$

Looking at equations (2.11) and (2.12), we can say that for a polyatomic systems like H_3^+ , the bond directionality principle holds true for each of the bonds. EMD exhibits a maximal nature perpendicular to each of the bonding direction. Thus we try to look at the pair-wise momentum densities for the polyatomic systems.

2.2.2 Variation of EMD with increasing bond length

Like H_2 , we tried plotting $\gamma(\vec{0})$ and Laplacian for H_2^+ at varying H-H bond length. The three H-H bonds were varied equally. Here also both RHF and full CI method was used along with an even-tempered extended coemd-ref basis set.

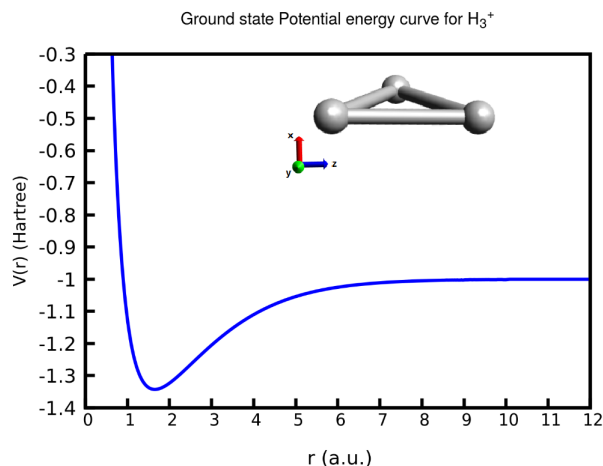


Fig. 2.4: Ground state potential energy curve for H_3^+ , calculated using full CI method with the extended coemd-ref basis set and RHF level of theory at each H-H bond length.

Fig.(2.4) shows the potential energy curve for the ground state of the H_3^+ molecule calculate using the full CI method at varying bond length. The EMD and laplacian at $|\vec{p}| = 0$ for each of these bond length was calculated using an in-house code for momentum space properties.

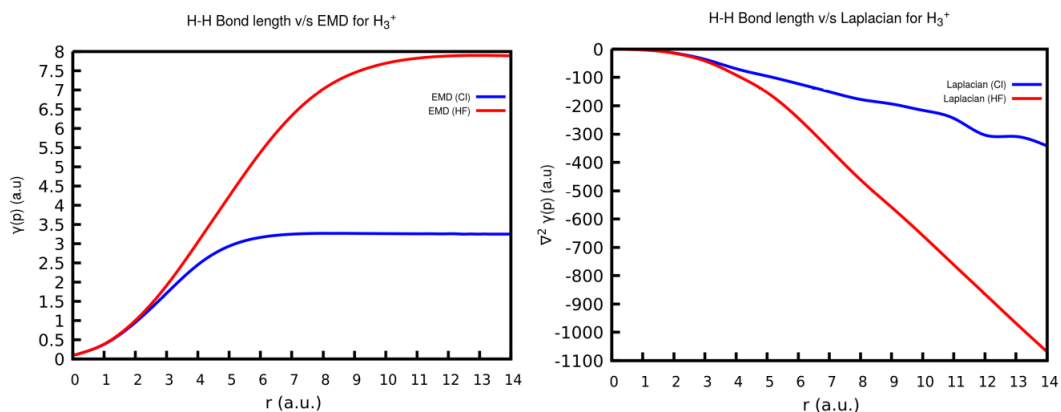


Fig. 2.5: A plot of (a) EMD and (b) Laplacian of EMD for H_3^+ at $|\vec{p}| = 0$ as a function of the bond length. The values of both EMD and Laplacian at $|\vec{p} = 0|$ was calculated using an in-house code for momentum space properties.

Fig.2.5(a) shows the variation of EMD at $|\vec{p}| = 0$ with increasing bond length. We can see from the curve for EMD that the value of $\gamma(\vec{0})$ increases with increasing bond-length in case of the RHF method. As we know, that the valence character of any system is observed at $|\vec{p}| = 0$. When $r = 0$, the two H atoms are strongly bonded and therefore have a very weak valence character, so the $\gamma(\vec{0})$ value is low

at low r . As r increases, the separation of the H atoms lead to an increase in the valence character, thereby increasing $\gamma(\vec{0})$. However, for the full CI method, we see that there's a sharp increase in the value of EMD initially but, gradually the value become constant with little to no change.

Fig.2.5(b) shows the variation of the Laplacian of the EMD at $|\vec{p}| = 0$ with increasing bond length. From the blue curve (full-CI) of the Laplacian we can see that when the values of $\langle 0 \rangle$ are increasing, the laplacian is far from zero. This is because the deviation at each point from the average values around that point is high. However, when the $\langle 0 \rangle$ values start converging, the laplacian gets closer to zero because the deviation is now almost negligible.

Bond length(a.u.)	0.05	1.045	1.704	2.043
HF Calculations Isoval = 0.00002				
Isovalue range	0 - 0.09955	0 - 0.404788	0 - 0.78467	0 - 1.03358
CI Calculations (NSOs) Isoval = 0.009				
Isovalue range	0.00153 - 0.09980	0.000155 - 0.39694	0.000026 - 0.75415	0.00002 - 0.97991

Bond length(a.u.)	3.039	4.036	5.032	6.029
HF Calculations Isoval = 0.00002				
Isovalue range	0 - 1.95316	0 - 3.08745	0 - 4.27645	0 - 5.40931
CI Calculations (NSOs) Isoval = 0.009				
Isovalue range	0.000043 - 1.74174	0.000016 - 2.47527	0.000025 - 2.94732	0.000036 - 3.16633

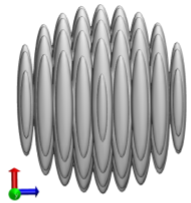
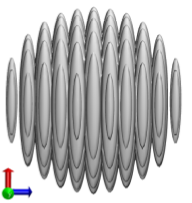
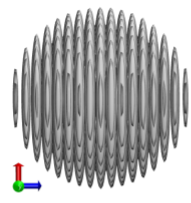
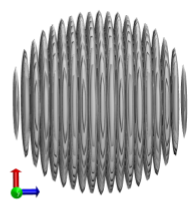
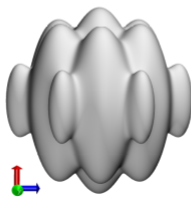
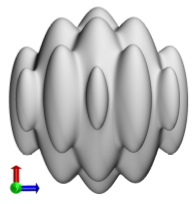
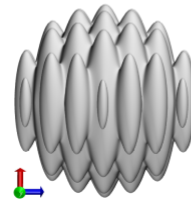
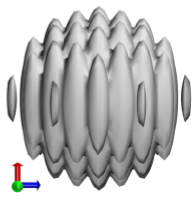
Bond length(a.u.)	7.025	8.022	12.008	15.994
HF Calculations Isoval = 0.00002				
Isovalue range	0 - 6.35307	0 - 7.03266	0 - 7.90756	0 - 7.9446
CI Calculations (NSOs) Isoval = 0.009				
Isovalue range	0.00004 - 3.24703	0.000035 - 3.26807	0.000042 - 3.25362	0 - 3.2468

Fig. 2.6: Isosurfaces of EMDs for H_3^+ at varying H-H bond length using the coemod-ref basis set along the restricted Hartree-Fock level of theory, visualized using VMD. The isovalues given in the figure are in a.u.

We've also tried plotting the isosurfaces for EMDs at varying bond lengths of 0.05 a.u. to 16 a.u., using both RHF and full CI method and tried comparing the isosurfaces from the two methods. From Fig.(2.6), we can see that when the separation between the atoms is small (0.05 - 1 a.u.), there are no oscillations and the isosurface also looks equivalent on all axes. As we move closer to the equilibrium bond length (~ 1.77 a.u.), we see that the maximal nature of the EMD is perpendicular to the position space bonding directions and the oscillations also start to set in. Upon an increase in the bond length, the number of oscillations also increases. This may be because at higher bond lengths, the atoms no longer remain bonded and have individual oscillations, and the number of these oscillations increase as the separation between the two H atoms. When the isosurfaces from the two methods are compared, we notice that in case of the full CI method, the oscillations start to set in much later than that of the RHF method.

2.3 Ethylene Molecule

In ethylene molecule, one of the three hybridised sp_2 orbital on each of the C atom overlaps to form the σ -bond and the p_z orbitals on each of the C atom overlap to form a π -bond. Both, σ and π bond in the system are on the same axis (bonding axis). We'll look at the contributions of these two bonds to the bond directionality in momentum space.

To look at the pi contribution, we can only look at the orbitals contributing to the pi-bond, i.e. $2p_z$ orbital. The molecular orbital for an electron forming part of the π bond between C_A and C_B can be written as:

$$\Psi(\vec{r}) = \frac{1}{\sqrt{2(1+S^2)}} [\psi_{2p_z}^A(\vec{r}) + \psi_{2p_z}^B(\vec{r})] \quad (2.13)$$

If $\psi_{2p_z}(\vec{r})$ is a Gaussian type orbital, then its Fourier transform gives the wavefunction in momentum space.

$$\phi_{p_z}(\vec{p}) = (-i)(2\pi\alpha)^{-\frac{3}{4}} \left(\frac{p_z}{\alpha^{\frac{1}{2}}} \right) \exp\{-i\vec{p} \cdot \vec{A}\} \exp\left\{ \frac{-p^2}{4\alpha} \right\} \quad (2.14)$$

$$\Phi(\vec{p}) = \frac{1}{\sqrt{2(1+S^2)}} [(-ip_z)e^{-i\vec{p} \cdot \vec{R}_A} + (-ip_z)e^{-i\vec{p} \cdot \vec{R}_B}] A(\vec{p}) \quad (2.15)$$

Momentum density can be given as:

$$\begin{aligned} |\Phi_\pi(\vec{p})|^2 &= \Phi(\vec{p})\Phi^*(\vec{p}) \\ &= \frac{1 + \cos \vec{p} \cdot (\vec{R}_A - \vec{R}_B)}{1 + S^2} p_z^2 |A(\vec{p})|^2 \end{aligned} \quad (2.16)$$

Now to look at the σ contribution, we look at sp_2 orbitals. The molecular orbital for an electron forming part of the σ bond between C_A and C_B can be written as:

$$\Psi(\vec{r}) = \frac{1}{\sqrt{2(1+S^2)}} [\psi_{sp_2}^A(\vec{r}) + \psi_{sp_2}^B(\vec{r})] \quad (2.17)$$

$$\psi_{sp_2} = c_1\psi_{2s} + c_2\psi_{2p_x} + c_3\psi_{2p_y} \quad (2.18)$$

$$\phi_s(\vec{p}) = (2\pi\alpha)^{-\frac{3}{4}} \exp\{-i\vec{p} \cdot \vec{A}\} \exp\left\{ \frac{-p^2}{4\alpha} \right\}$$

$$\phi_{p_x}(\vec{p}) = (-i)(2\pi\alpha)^{-\frac{3}{4}} \left(\frac{p_x}{\alpha^{\frac{1}{2}}} \right) \exp\{-i\vec{p} \cdot \vec{A}\} \exp\left\{ \frac{-p^2}{4\alpha} \right\}$$

Therefore,

$$\Phi_\sigma(\vec{p}) = \frac{1}{\sqrt{2(1+S^2)}} [\{e^{-i\vec{p}\cdot\vec{R}_A} + (-ip_x)e^{-i\vec{p}\cdot\vec{R}_A} + (-ip_y)e^{-i\vec{p}\cdot\vec{R}_A}\} + \{e^{-i\vec{p}\cdot\vec{R}_B} + (-ip_x)e^{-i\vec{p}\cdot\vec{R}_B} + (-ip_y)e^{-i\vec{p}\cdot\vec{R}_B}\}] A(\vec{p}) \quad (2.19)$$

Momentum density can then be calculated as:

$$|\Phi_\sigma(\vec{p})|^2 = \Phi(\vec{p})\Phi^*(\vec{p}) \quad (2.20)$$

On substituting $\Phi_\sigma(\vec{p})$ from eqn.(2.19) and its conjugate, in eqn(2.20) we get the following:

$$|\Phi_\sigma(\vec{p})|^2 = \frac{1 + \cos \vec{p}\cdot(\vec{R}_A - \vec{R}_B)}{1 + S^2} \{1 + p_x^2 + p_y^2 + 2p_x p_y\} |A(\vec{p})|^2$$

Hence the total contribution from both, σ and π bonds, is given as:

$$\begin{aligned} \gamma(\vec{p}) &= |\Phi_\sigma(\vec{p})|^2 + |\Phi_\pi(\vec{p})|^2 \\ &= \frac{1 + \cos \vec{p}\cdot(\vec{R}_A - \vec{R}_B)}{1 + S^2} \{1 + p_x^2 + p_y^2 + p_z^2 + 2p_x p_y\} |A(\vec{p})|^2 \end{aligned} \quad (2.21)$$

2.4 Bond-Oscillation Principle

From the equation:

$$\gamma(\vec{p}) = \frac{1 + \cos \vec{p}\cdot(\vec{R}_A - \vec{R}_B)}{1 + S} |A(\vec{p})|^2 \quad (2.22)$$

we can see that the geometry information about the equilibrium nuclear positions (\vec{R}_A , \vec{R}_B , etc.) is included only in the diffraction factor, *i.e.*, the \cos term, introduced by Fourier transformation of the position space wavefunction to the momentum space wave function. Thus the electron momentum distribution is modulated by a cosine function with a periodicity of $\frac{2\pi}{|\vec{R}_A - \vec{R}_B|}$. This oscillation induced by the diffraction term is referred to as the **bond-oscillation principle**.

2.5 Pair-wise momentum densities

From the analytical expression of $\gamma(\vec{p})$ for H_3^+ (eqn. 2.12), we concluded that to understand the bond-directionality principle in polyatomic system we need to look

at pair-wise momentum densities.

$$\Phi_a(\vec{p}) = \sum_{\mu=1}^k c_{\mu a} \varphi_{\mu}(\vec{p}) \quad (2.23)$$

$$\varphi_{\mu}(\vec{p}) = \sum c_i \phi_{i\mu}(\vec{p}) \quad (2.24)$$

$$\phi_{i\mu}(\vec{p}) = n_{iA} \chi_{iA\mu}(\vec{p}) \quad (2.25)$$

$$\begin{aligned} \chi_{iA\mu}(\vec{p}) = & \sum_{k_1=0}^{[l/2]} \frac{(-1)^{k_1} (p_x/\sqrt{\alpha})^{l-2k_1}}{k_1!(l-2k_1)!} \sum_{k_2=0}^{[m/2]} \frac{(-1)^{k_2} (p_y/\sqrt{\alpha})^{m-2k_2}}{k_2!(m-2k_2)!} \\ & \sum_{k_3=0}^{[n/2]} \frac{(-1)^{k_3} (p_z/\sqrt{\alpha})^{n-2k_3}}{k_3!(n-2k_3)!} \exp\left(-\left(\frac{p^2}{4\alpha} + i\vec{p} \cdot \vec{A}\right)\right) \end{aligned} \quad (2.26)$$

$$\begin{aligned} \gamma(\vec{p}) &= \Phi_i^*(\vec{p}) \Phi_i(\vec{p}) = \sum_{\mu} c_{\mu a}^* \varphi_{\mu}^*(\vec{p}) \sum_{\nu} c_{\nu a} \varphi_{\nu}(\vec{p}) \\ &= \sum_{\mu, \nu} (2 \sum_a c_{\mu a}^* c_{\nu a}) \varphi_{\mu}^*(\vec{p}) \varphi_{\nu}(\vec{p}) \\ &= \sum_{\mu, \nu} P_{\mu\nu} (\sum_i c_i \phi_{i\mu}(\vec{p}))^* (\sum_j c_j \phi_{j\nu}(\vec{p})) \\ &= \sum_{\mu, \nu} P_{\mu\nu} \sum_i \sum_j c_i^* c_j n_{iA}^* n_{jA} \chi_{iA\mu}^* \chi_{jA\nu} \end{aligned}$$

$$\begin{aligned} \gamma(\vec{p}) = & \sum_{\mu, \nu} P_{\mu\nu} \sum_i \sum_j c_i^* c_j n_{iA}^* n_{jA} \left\{ \sum_{k_1=0}^{[l_{\mu}/2]} \frac{(-1)^{k_1} (p_x/\sqrt{\alpha})^{l_{\mu}-2k_1}}{k_1!(l_{\mu}-2k_1)!} \right. \\ & \sum_{k_2=0}^{[m_{\mu}/2]} \frac{(-1)^{k_2} (p_y/\sqrt{\alpha})^{m_{\mu}-2k_2}}{k_2!(m_{\mu}-2k_2)!} \sum_{k_3=0}^{[n_{\mu}/2]} \frac{(-1)^{k_3} (p_z/\sqrt{\alpha})^{n_{\mu}-2k_3}}{k_3!(n_{\mu}-2k_3)!} \Big\} \\ & \left\{ \sum_{k_1=0}^{[l_{\nu}/2]} \frac{(-1)^{k_1} (p_x/\sqrt{\alpha})^{l_{\nu}-2k_1}}{k_1!(l_{\nu}-2k_1)!} \sum_{k_2=0}^{[m_{\nu}/2]} \frac{(-1)^{k_2} (p_y/\sqrt{\alpha})^{m_{\nu}-2k_2}}{k_2!(m_{\nu}-2k_2)!} \right. \\ & \left. \sum_{k_3=0}^{[n_{\nu}/2]} \frac{(-1)^{k_3} (p_z/\sqrt{\alpha})^{n_{\nu}-2k_3}}{k_3!(n_{\nu}-2k_3)!} \right\} e^{(-\frac{p^2}{4} (\frac{1}{\alpha_{\mu}} - \frac{1}{\alpha_{\nu}}))} e^{(i\vec{p} \cdot (\vec{A}_{\mu} - \vec{A}_{\nu}))} \end{aligned} \quad (2.27)$$

If $\mu \in$ atom centre A and $\nu \in$ atom centre B then we can have the pair wise momentum densities.

2.5.1 Pair-wise momentum densities for H_3^+

From Fig. 2.7(a), we can see that the total electron momentum density of the system is maximal in the direction perpendicular to the molecular system, which is in accordance with the *bond-directionality principle*. The pair-wise momentum densities of the H-H bonds are shown in Fig. 2.7(c), which shows that the pairwise densities are maximum in a direction along each of these bonds. However, they stretch along a direction perpendicular to the bond, *i.e.*, they are wider in a direction perpendicular to the bond. This is in accordance with the bond-directionality principle. The values of these pair-wise densities range from -ve to +ve through zero and these oscillations are parallel the bonding direction. This is in accordance with the *bond-oscillation principle*.

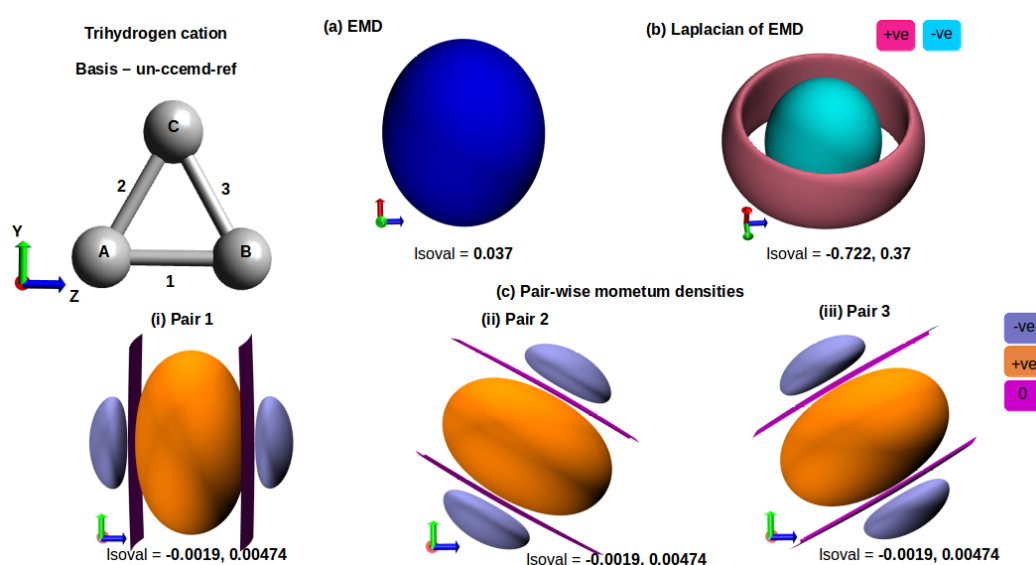


Fig. 2.7: (a) Isosurface for the total momentum density, (b) Isosurface of the Laplacian of the EMD and (c) Isosurfaces for the pairwise momentum densities of different pairs of H_3^+ . All the given isovalues are in a.u.

2.5.2 Pair-wise momentum densities for Water

From fig. 2.8(a), we can see that the total electron momentum density of the system is maximal in the direction perpendicular to the molecular system, which is in accordance with the *bond-directionality principle*. The pair-wise momentum densities of different pairs are shown in fig. 2.8(c), which shows that the pairwise densities are maximum in a direction along each of these bonds. However, they stretch along a direction perpendicular to the bond, *i.e.*, they are wider in a direction perpendicular

to the bond. This is in accordance with the bond-directionality principle. The values of these pair-wise densities range from -ve to +ve through zero and these oscillations are parallel the bonding direction. This is in accordance with the *bond-oscillation principle*.

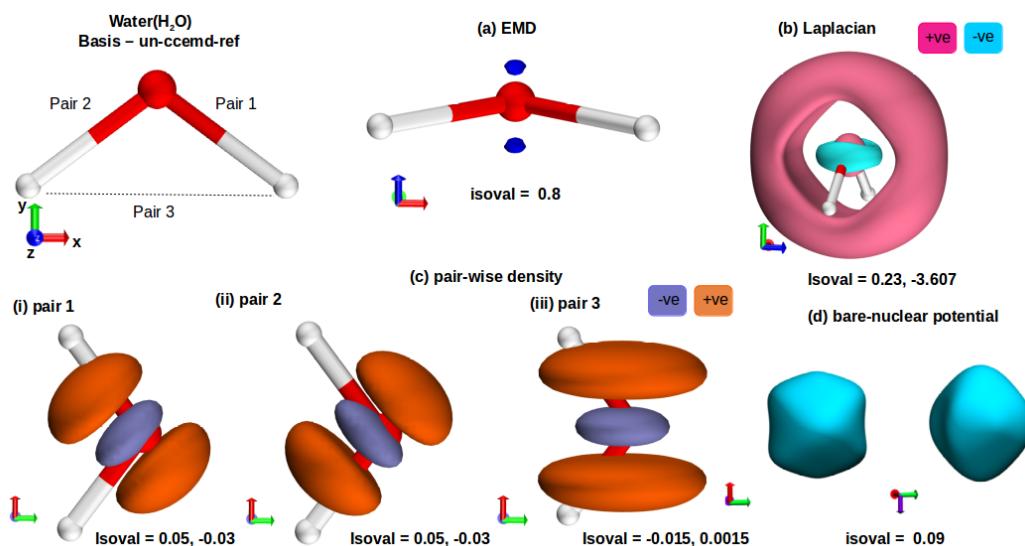


Fig. 2.8: (a) Isosurface for the total momentum density, (b) Isosurface of the Laplacian of the EMD, (c) Isosurfaces for the pairwise momentum densities of different pairs and (d) Isosurface of the bare-nuclear potential of H_2O . All the given isovalues are in a.u.

2.5.3 Pair-wise densities for Ethylene

From fig. 2.9(a), we can see that the total electron momentum density of the system is maximal in the direction perpendicular to the molecular system, which is in accordance with the *bond-directionality principle*. The pair-wise momentum densities of different pairs are shown in fig. 2.9(c), which shows that the pairwise densities are maximum in a direction along each of these bonds. However, they stretch along a direction perpendicular to the bond, *i.e.*, they are wider in a direction perpendicular to the bond. This is in accordance with the bond-directionality principle. The values of these pair-wise densities range from -ve to +ve through zero and these oscillations are parallel the bonding direction. This is in accordance with the *bond-oscillation principle*.

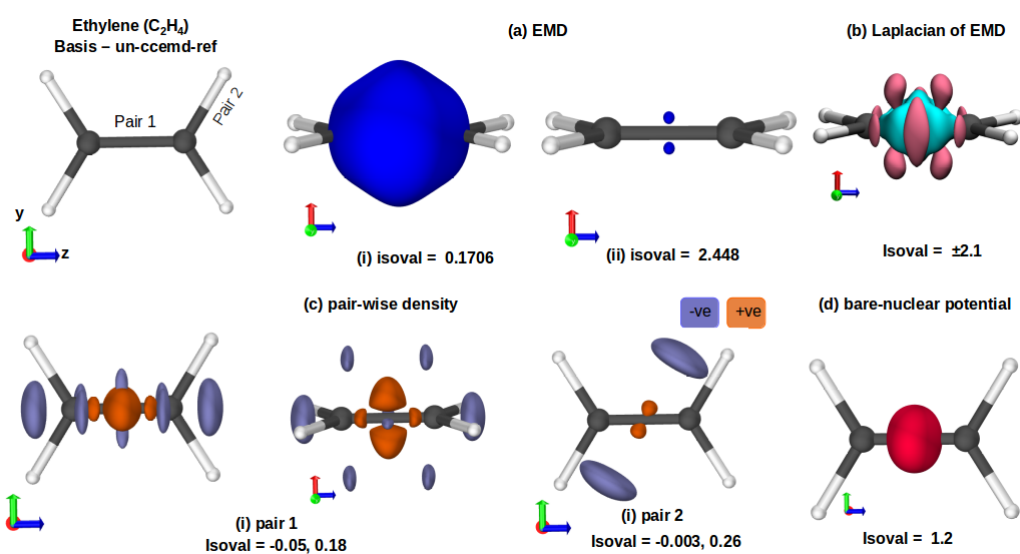


Fig. 2.9: (a) Isosurface for the total momentum density, (b) Isosurface of the Laplacian of the EMD, (c) Isosurfaces for the pairwise momentum densities of different pairs and (d) Isosurface of the bare-nuclear potential of C_2H_4 . All the given isovalues are in a.u.

Molecular Electron Momentum Densities of Field-dressed Systems

This chapter discusses bond-directionality of the above-studied systems in presence of an external oscillating electric field. The influence of an external field on various chemical processes have been studied in the past [1][2]. Recently M. Paul *et. al.* [3] studied the rotatory response of EMDs in presence of a linear, homogenous, weak electric field.

The advancement in laser technology has made possible, the study of the interaction of atoms and molecules with fields of intensities of the order of 10^{14} W/cm² - 10^{15} W/cm². Some of the interesting phenomena observed under such high intensities include multi-photon ionization, tunnel ionization and barrier suppression ionization.

In this thesis we have approximated a cosine function as the intense laser that perturbs our system. Since the laser is a periodic perturbation, there exist a method to solve periodic hamiltonians. Floquet method, introduced by Shirley [4], enables us to represent the time-dependent Hamiltonian to be represented as a time-independent infinite matrix. A unitary transformation provides us with some solutions and describes the evolution in time for any general wavefunction.

$$\psi_n(\vec{r}, t) = e^{\frac{-iE_n t}{\hbar}} \phi_n(\vec{r}, t) \quad (3.1)$$

Plugging in the unitary transformed wavefunction to the time dependent Schrödinger equation we obtain a new Hamiltonian of the form $H_F(r, t) = -i\hbar \frac{\partial}{\partial t} + \hat{H}(r, t)$ and the TDSE now looks like

$$\hat{H}_F(\vec{r}, t) \phi_n(\vec{r}, t) = E_n \phi_n(\vec{r}, t) \quad (3.2)$$

The general solution to the above equation can be written as

$$\psi(\vec{r}, t) = \sum_{n=-\infty}^{\infty} a_n e^{\frac{-iE_n t}{\hbar}} \phi_n(\vec{r}, t) \quad (3.3)$$

To solve for the wavefunction we use (t,t') method devised and developed by Peskin and Moiseyev. The (t,t') method brings in a new dimension t' to the wavefunction in an extended Hilbert space as suggested by Sambe and Howland, such that the TDSE becomes:

$$i\hbar \left[\frac{\partial}{\partial t} + \frac{\partial}{\partial t'} \right] \tilde{\Psi}(\vec{r}, t, t') = \hat{H}_F(\vec{r}, t') \tilde{\Psi}(\vec{r}, t, t') \quad (3.4)$$

An in-house code for the (t,t') method has been used for looking at the time-dependent momentum densities of different systems.

3.1 Complex Absorbing Potential (CAP)

The evolution of wave packets is usually carried out using discrete representation of the Hamiltonian and the wave function in a finite grid. However, in scattering processes the wave moves towards some outgoing asymptotic state where the effect of the interaction or parts of it vanish because one or more coordinates tend to infinity. The spatially finite grid box cannot represent this process indefinitely because the leading part of the wave will eventually arrive at the box edge and be reflected. The reflected parts of the wave may spoil the physical validity of the calculation due to the interference with the part of the wave remaining in the box. Enlarging the box size delays the interferences, so that the desired quantities (transition probabilities, life times) may be obtained, at the price of a considerable increase of computing time. Another effective way is the addition of a **Complex Absorbing Potential (CAP)** [5] at the box edge. The grid should be large enough to span the range of coordinates over which the potential is important. The complex potential should absorb the wave completely in a small length without modifying the physical wave function in the inner part of the grid, and be numerically robust with respect to discretization.

3.2 Results and Discussion

A molecular system in presence of an intense electric field, usually, undergoes ionisation, which means that a valence electron escapes the system and goes to an infinite distance. We'll, therefore, be looking at the variation in EMD values at $\vec{p} = 0$ with varying electric field.

In field free systems, we have seen that $\gamma(\vec{0})$ can be maximum (in case of H_2), as well as minimum (in case of H_3^+). So, if a molecule undergoes ionisation in presence of

a laser, how can we account for it using the $\gamma(\vec{0})$. We'll try to see if the ionisation can be accounted by $\gamma(\vec{0}) = 0$.

3.2.1 H_2

For H_2 , we used the coemd-ref basis set. Laser was polarized in Z-direction, *i.e.* the bonding direction, with intensity, $\epsilon = 0.25$ a.u. $= 0.219 \times 10^{16}$ W/cm² and frequency, $\omega = 0.21$ a.u. $= 5.714$ eV, for 12 optical cycles, out of which the number of optical cycles for rising pulse, CW region pulse and descending pulse is 2 each. And, the CAP box size is set to 20,26,26. From fig.(3.1) we can see that the norm decreases and then converges, which means that ionisation of the valence electron of H_2 takes place. Also, The $\gamma(\vec{0})$ values go to zero. A possible reason for this may be that due to ionization, the valence electron goes to infinity and thus $\gamma(\vec{0})$ goes to 0.

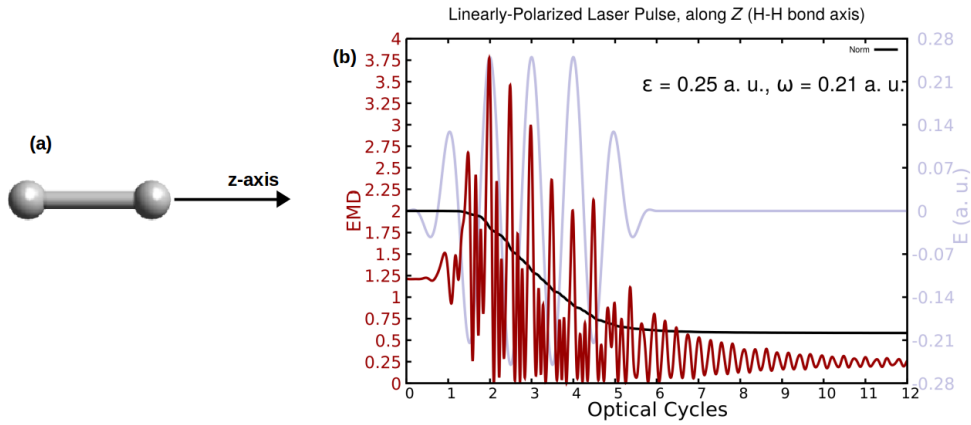


Fig. 3.1: (a) Geometry of H_2 molecule. The black arrow denotes the direction in which the laser is induced. (b) Variation of $\gamma(\vec{0})$ with optical cycle in the presence of a linearly polarized Laser, along Z-direction. The x-axis represents the no. of optical cycles and the y1- and y2- axis represent EMD, $\gamma(\vec{0})$ (in red) and the energy of the pulse (in purple) in a.u., respectively. The electric field runs for 12 optical cycles and the pulse is ended after the 6th optical cycle, with intensity, $\epsilon = 0.25$ a.u., $\omega = 0.21$ a.u., quiver distance, $\alpha_o = 5.668934$ a.u., with the CAP box size set to 20,26,26

Fig.(3.2) shows the variation of the laplacian, $\nabla^2\gamma(\vec{0})$, of EMD with optical cycle in the presence of a linearly polarized Laser, along Z-direction. The Laplacian, here, seems to show a trend. It dips to most negative at peak field strengths and most positive when the pulse is zero. The positive Laplacian sustains when the pulse is switched off.

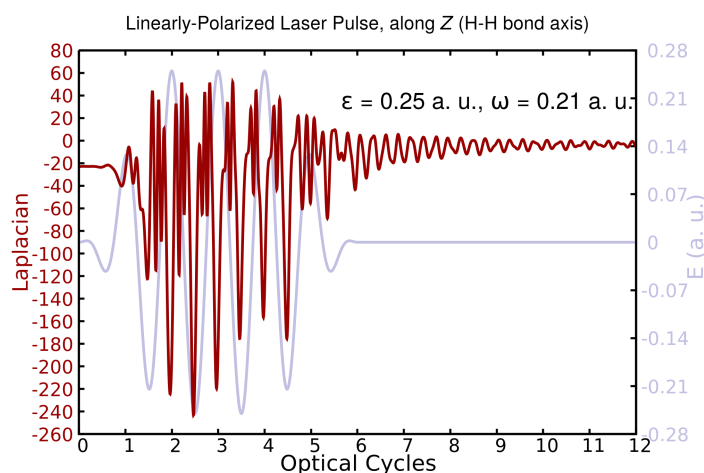


Fig. 3.2: Variation of the laplacian, $\nabla^2\gamma(\vec{0})$, of EMD for H_2 , with optical cycle in the presence of a linearly polarized Laser, along Z-direction. The x-axis represents the no. of optical cycles and the y1- and y2- axis represent $\nabla^2\gamma(\vec{0})$ (in red) and the energy of the pulse (in purple) in a.u., respectively and intensity, $\epsilon = 0.25a.u.$

3.2.2 H_3^+

For H_3^+ , we have tried to look at the behaviour of $\gamma(\vec{0})$ in presence of linearly-polarized lasers, along all three directions, X, Y and Z, and with different intensities (0.25, 0.75). We also calculated the transition dipole moments for H_3^+ in all three directions. A transition from orbital 1 (HOMO) to orbital 3 was observed for Z polarization. Higher orbital transitions were not so significant in case of X and Y polarization.

For the first set of calculations, we used un-ccemd-ref basis set to carry out the time propagation calculation and the laser was set along the X-direction (perpendicular to the molecular plane) with intensity, $\epsilon = 0.25 \text{ a.u.} = 0.219 \times 10^{16} \text{ W/cm}^2$ and $\epsilon = 0.75 \text{ a.u.} = 1.974 \times 10^{16} \text{ W/cm}^2$, and frequency, $\omega = 0.21 \text{ a.u.} = 5.714 \text{ eV}$, for 12 optical cycles, out of which the number of optical cycles for rising pulse, CW region pulse and descending pulse is 2 each.

From Fig.(3.3), we observe that the norm is conserved throughout when the laser polarisation is along the X axis, even at higher intensity of the field which indicates that there's no ionisation taking place. Also, the $\gamma(\vec{0})$ values do not go to zero at any point in time. However, in presence of a strong field, the variation in values of $\gamma(\vec{0})$ is very high compared to what was observed in the case of field with lower intensity.

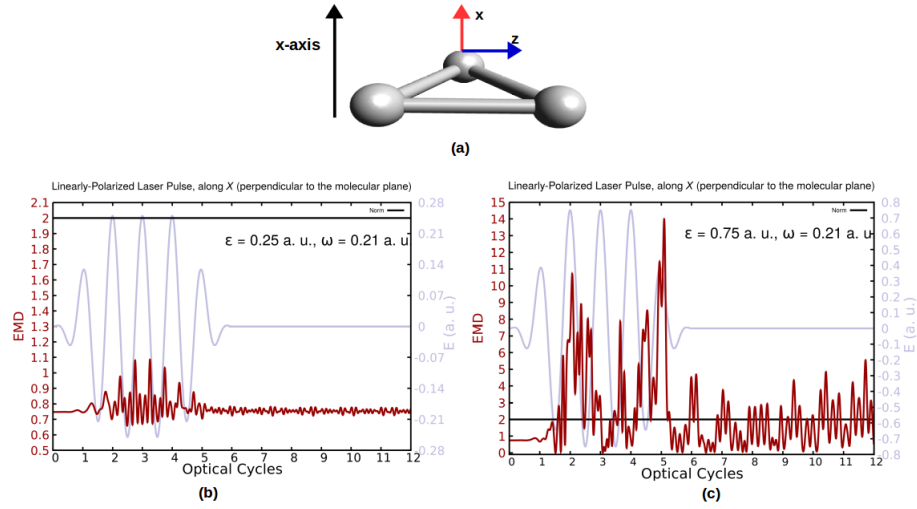


Fig. 3.3: (a) Geometry of H_3^+ molecule. The black arrow denotes the direction in which the laser is induced. (b) Variation of $\gamma(\vec{0})$ with optical cycle in the presence of a linearly polarized Laser, along X-direction. The x-axis represents the no. of optical cycles and the y1- and y2- axis represent EMD, $\gamma(\vec{0})$ (in red) and the energy of the pulse (in purple) in a.u., respectively. The electric field runs for 12 optical cycles and the pulse is ended after the 6th optical cycle, with intensity, $\epsilon = 0.25$ a.u., $\omega = 0.21$ a.u., quiver distance, $\alpha_o = 5.668934$ a.u., and (c) with intensity, $\epsilon = 0.75$ a.u., $\omega = 0.21$ a.u., quiver distance, $\alpha_o = 17.007$ a.u., with the CAP box size set to 10,15,15.

Fig.3.4(a) and (b) shows the variation of the laplacian, $\nabla^2\gamma(\vec{0})$, of EMD with optical cycle in the presence of a linearly polarized Laser, along X-direction at intensities with intensities 0.25 and 0.75, respectively.

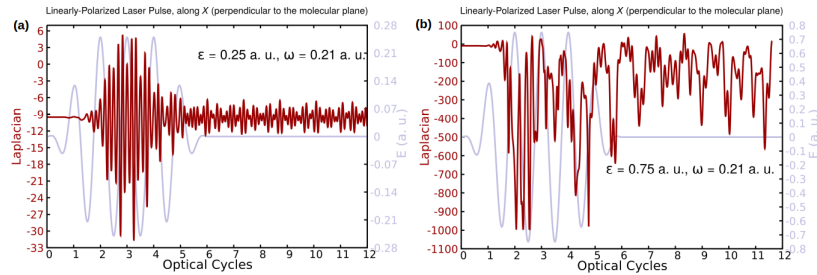


Fig. 3.4: Variation of the laplacian, $\nabla^2\gamma(\vec{0})$, of EMD for H_3^+ , with optical cycle in the presence of a linearly polarized Laser, along X-direction. The x-axis represents the no. of optical cycles and the y1- and y2- axis represent $\nabla^2\gamma(\vec{0})$ (in red) and the energy of the pulse (in purple) in a.u., respectively. (a) Intensity, $\epsilon = 0.25$ a.u. and (b) Intensity, $\epsilon = 0.75$ a.u.

Next, we tried putting the laser along Y- and Z-direction (parallel to the molecular plane). Fig.(3.5), shows the variation of $\gamma(\vec{0})$ with optical cycles. The norm remains unchanged even in this case and $\gamma(\vec{0})$ does not become zero.

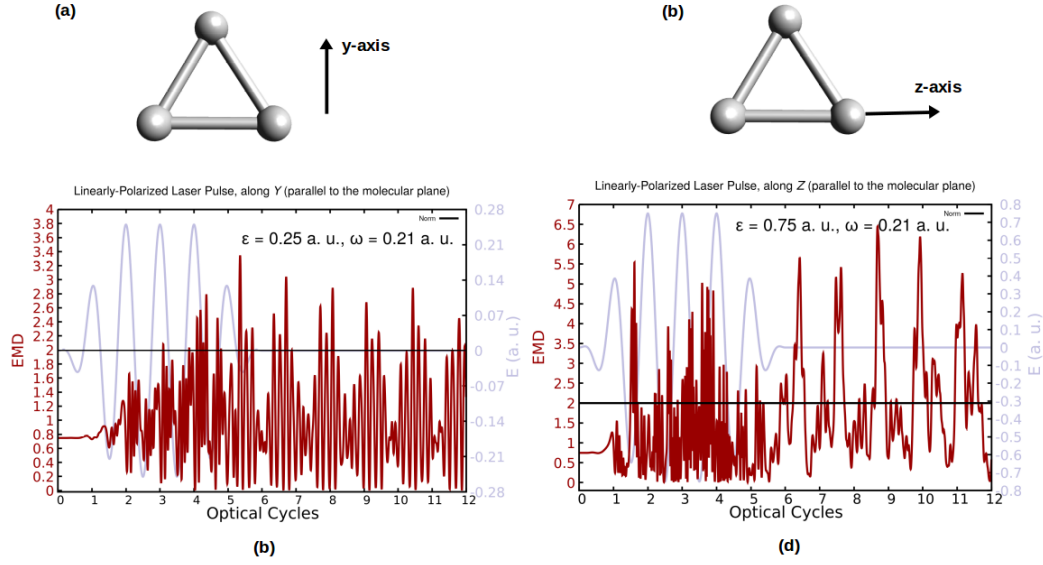


Fig. 3.5: (a),(b) Geometry of H_3^+ molecule. The black arrows denotes the direction in which the laser is induced. (c) Variation of $\gamma(\vec{0})$ with optical cycle. The x-axis represents the no. of optical cycles and the y1- and y2- axis represent EMD, $\gamma(\vec{0})$ (in red) and the energy of the pulse (in purple) in a.u., respectively. The electric field runs for 12 optical cycles and the pulse is ended after the 6th optical cycle with polarization along Y-direction with intensity, $\epsilon = 0.25$ a.u., $\omega = 0.21$ a.u., quiver distance, $\alpha_o = 5.668934$ a.u. and the CAP box size is set to 20,26,26 and (d) with polarization along Z-direction with intensity, $\epsilon = 0.75$ a.u., $\omega = 0.21$ a.u., quiver distance, $\alpha_o = 17.007$ a.u. and the CAP box size is set to 20,26,26.

Fig.3.6 (a) and (b) shows the variation of the laplacian, $\nabla^2\gamma(\vec{0})$, of EMD with optical cycle in the presence of a linearly polarized Laser, along Y-direction with $\epsilon = 0.25$ and along Z-direction with $\epsilon = 0.75$, respectively.

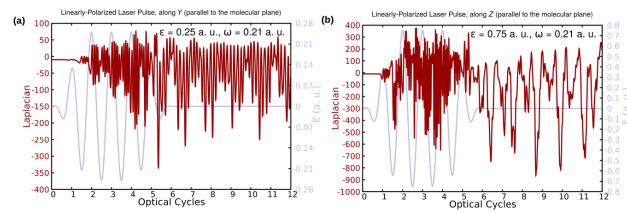


Fig. 3.6: Variation of the laplacian, $\nabla^2\gamma(\vec{0})$, of EMD for H_3^+ , with optical cycle in the presence of a linearly polarized Laser, along (a) Y-direction with $\epsilon = 0.25$ a.u. and (b) along Z-direction with $\epsilon = 0.75$ a.u. The x-axis represents the no. of optical cycles and the y1- and y2- axis represent $\nabla^2\gamma(\vec{0})$ (in red) and the energy of the pulse (in purple) in a.u., respectively.

3.2.3 Water (H₂O)

For water, we used the aug-cc-pVDZ basis set with extra *s*- functions on oxygen. Here, a transition from orbital 5 (HOMO) to a higher orbital, orbital 12 was observed for Z polarization. However for X and Y polarization, no significant transitions were observed.

The laser was polarized in Z-direction, *i.e.*, parallel to the molecular plane with intensity, $\epsilon = 0.25$ a.u. = 0.219×10^{16} W/cm² and frequency, $\omega = 0.21$ a.u. = 5.714 eV, for 12 optical cycles, out of which the number of optical cycles for starting pulse, CW region pulse and end pulse is 2 each. And, the CAP box size is set to 10,20,20. From fig.(3.7) we can see that the norm is decreasing and converging, implying ionisation. But, the $\gamma(\vec{0})$ values does not go to zero, even though there's ionisation. {Interpretation not very clear, has to be written}

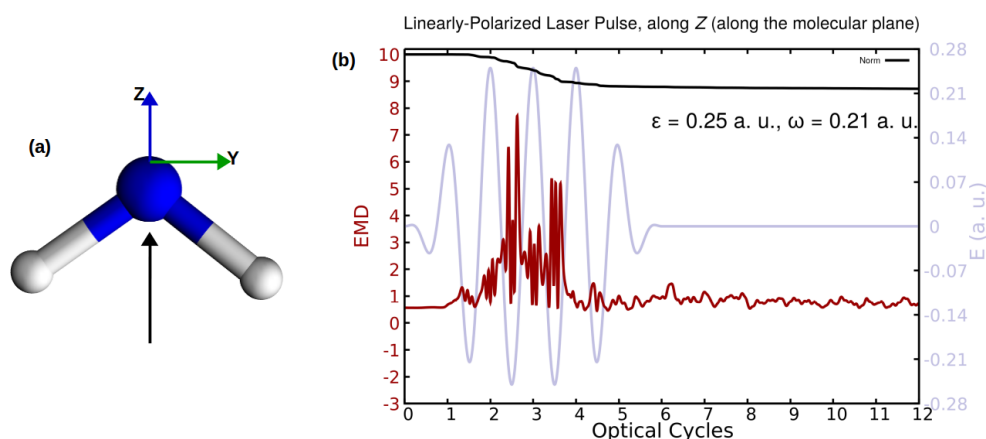


Fig. 3.7: (a) Geometry of H₂O molecule. The black arrow denotes the direction in which the laser is induced. (b) Variation of $\gamma(\vec{0})$ with optical cycle in the presence of a linearly polarized Laser, along Z-direction. The x-axis represents the no. of optical cycles and the y1- and y2- axis represent EMD, $\gamma(\vec{0})$ (in red) and the energy of the pulse (in purple) in a.u., respectively. The electric field runs for 12 optical cycles and the pulse is ended after the 6th optical cycle, with intensity, $\epsilon = 0.25$ a.u., $\omega = 0.21$ a.u., quiver distance, $\alpha_o = 5.668934$ a.u., with the CAP box size set to 10,20,20.

Fig.(3.8) shows the variation of the laplacian, $\nabla^2\gamma(\vec{0})$, of EMD with optical cycle in the presence of a linearly polarized Laser, along Z-direction for water. The Laplacian, here, seems to show a trend. It dips to most negative and most positive at peak field strengths and the positive Laplacian sustains when the pulse is switched off.

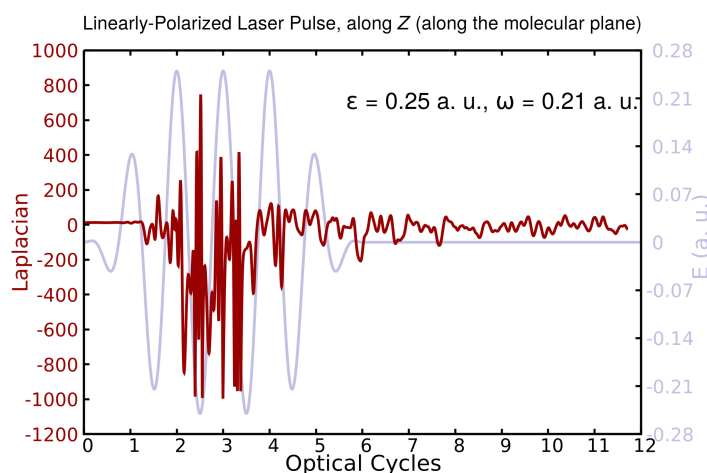


Fig. 3.8: Variation of the laplacian, $\nabla^2\gamma(\vec{0})$, of EMD for H_2O , with optical cycle in the presence of a linearly polarized Laser, along Z-direction. The x-axis represents the no. of optical cycles and the y1- and y2- axis represent $\nabla^2\gamma(\vec{0})$ (in red) and the energy of the pulse (in purple) in a.u., respectively and intensity, $\epsilon = 0.25a.u.$

3.2.4 Ethylene (C_2H_4)

For Ethylene, we used the aug-cc-pVDZ basis set. Upon calculating the transition dipole moments for ethylene, we see that there's a transition from HOMO (orbital 8) to higher orbitals (14, 25, etc.) for Y and Z polarisation, with transitions being more significant for Z as compared to that of Y.

Laser was first polarized in Z-direction, *i.e.*, parallel to the molecular plane with intensity, $\epsilon = 0.25 \text{ a.u.} = 0.219 \times 10^{16} \text{ W/cm}^2$ and frequency, $\omega = 0.21 \text{ a.u} = 5.714 \text{ eV}$, for 12 optical cycles, out of which the number of optical cycles for starting pulse, CW region pulse and end pulse is 2 each. And, the CAP box size is set to 10,20,20. The norm doesn't decrease significantly. However, when the Laser with intensity 0.75 a.u. is used the norm decreases significantly but does not converge after 12 cycles (Fig.3.9).

Fig.3.10 (a) and (b) shows the variation of the laplacian, $\nabla^2\gamma(\vec{0})$, of EMD with optical cycle in the presence of a linearly polarized Laser, along Z-direction with intensities 0.25 and 0.75, respectively.

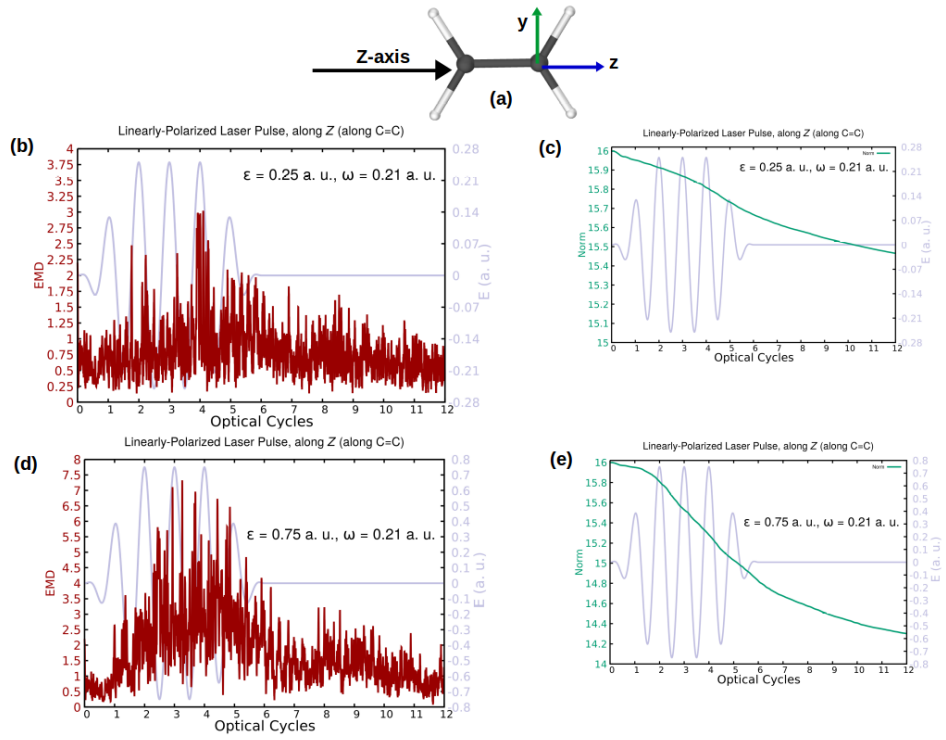


Fig. 3.9: (a) Geometry of C_2H_4 molecule. The black arrow denotes the direction in which the laser is induced. (b) Variation of $\gamma(\vec{0})$ with optical cycle in the presence of a linearly polarized Laser, along Z-direction. The x-axis represents the no. of optical cycles and the y1- and y2- axis represent EMD, $\gamma(\vec{0})$ (in red) and the energy of the pulse (in purple) in a.u., respectively. The electric field runs for 12 optical cycles and the pulse is ended after the 6th optical cycle, with intensity, $\epsilon = 0.25$ a.u., $\omega = 0.21$ a.u., quiver distance, $\alpha_o = 5.668934$ a.u. and (d) with intensity, $\epsilon = 0.75$ a.u., $\omega = 0.21$ a.u., quiver distance, $\alpha_o = 17.007$ a.u., with the CAP box size set to 10,15,20. And, (c) and (e) shows the norms for (b) and (d) respectively.

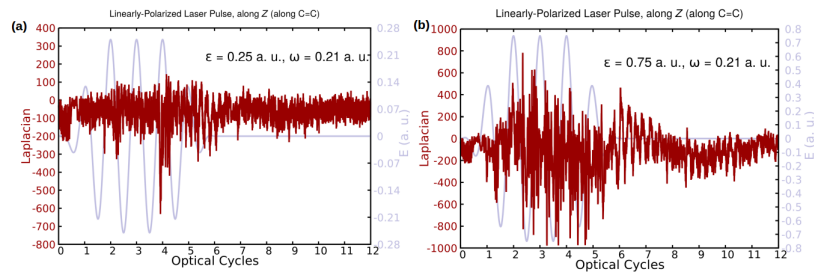


Fig. 3.10: Variation of the laplacian, $\nabla^2\gamma(\vec{0})$, of EMD for C_2H_4 , with optical cycle in the presence of a linearly polarized Laser, along Z-direction with intensities (a) 0.25 a.u. and (b) 0.75 a.u. The x-axis represents the no. of optical cycles and the y1- and y2- axis represent $\nabla^2\gamma(\vec{0})$ (in red) and the energy of the pulse (in purple) in a.u., respectively.

Next we applied the electric field along the Y-direction (perpendicular to C=C, Fig.3.11). We can see that the norm decreases significantly but does not converge after 12 cycles. And, the $\gamma(\vec{0})$ does not go to zero.

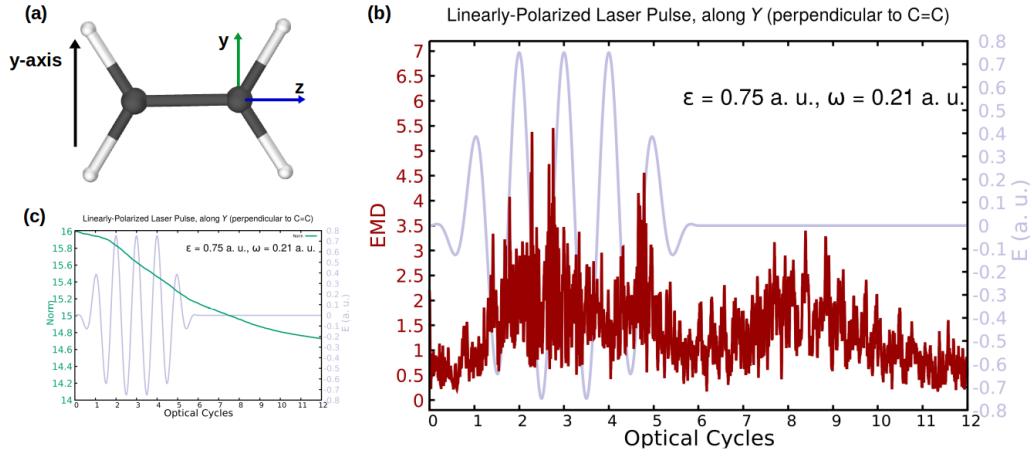


Fig. 3.11: (a) Geometry of C₂H₄ molecule. The black arrow denotes the direction in which the laser is induced. (b) Variation of $\gamma(\vec{0})$ with optical cycle in the presence of a linearly polarized Laser, along Z-direction. The x-axis represents the no. of optical cycles and the y1- and y2- axis represent EMD, $\gamma(\vec{0})$ (in red) and the energy of the pulse (in purple) in a.u., respectively. The electric field runs for 12 optical cycles and the pulse is ended after the 6th optical cycle, with intensity, $\epsilon = 0.25$ a.u., $\omega = 0.21$ a.u., quiver distance, $\alpha_o = 5.668934$ a.u. with the CAP box size set to 10,15,20. (c) Norm versus optical cycle.

Fig.3.12 shows the variation of the laplacian, $\nabla^2\gamma(\vec{0})$, of EMD with optical cycle in the presence of a linearly polarized Laser, along Y-direction with intensity 0.75.

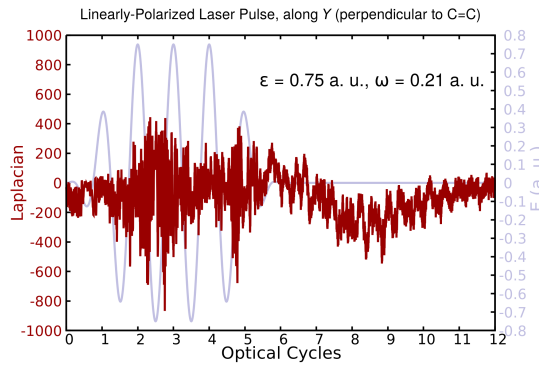


Fig. 3.12: Variation of the laplacian, $\nabla^2\gamma(\vec{0})$, of EMD for C₂H₄, with optical cycle in the presence of a linearly polarized Laser, along Y-direction with intensity 0.75 a.u. The x-axis represents the no. of optical cycles and the y1- and y2- axis represent $\nabla^2\gamma(\vec{0})$ (in red) and the energy of the pulse (in purple) in a.u., respectively.

3.3 Conclusion and Future Prospects

In chapter 3, We see a very clean relationship between change in the bond length in r -space and the change in number of oscillations in the EMD in p -space. Also, it is seen that for polyatomic systems, apart from the total EMD, the pairwise momentum densities should also be taken into account to explain the bond-directionality principle.

In this chapter, we see that in presence of an oscillating electric field, we see that the values for $\gamma(\vec{0})$ peaks at peak field strength and oscillates between a fixed value even when the pulse is turned off.

We can look at the first and second moments of the EMD, which are experimentally measurable. They'll tell us about the electronic phenomenon like ionisation.

References

- [1] N. D. Gurav, S. P. Gejji, L. J. Bartolotti, R. K. Pathak, *J. Chem. Phys.* **145**, 074302 (2016).
- [2] N. D. Gurav, A. D. Kulkarni, S. P. Gejji, R. K. Pathak, *J. Chem. Phys.* **142**, 214309 (2015).
- [3] M. Paul, R. K. Pathak, P. Balanarayan, *J. Phys. Chem. A* **124**, 943–954 (2019).
- [4] J.H. Shirley, *Phys. Rev. A*, **138**, 979-987 (1965).
- [5] J. G. Mugaa, J. P. Palaob, B. Navarroa, I. L. Egusquizac, *Phys. Reports*, **395**, 357-426 (2004).

